

“Nothing in life is to be feared, it is only to be understood. Now is the time to understand more, so that we may fear less.”

Marie Curie

University of Alberta

Modelling and MPC for a Primary Gas Reformer

by

Lei Sun

A thesis submitted to the Faculty of Graduate Studies and Research
in partial fulfillment of the requirements for the degree of

Master of Science

in

Process Control

Department of Chemical and Materials Engineering

©Lei Sun

Spring 2013

Edmonton, Alberta

Permission is hereby granted to the University of Alberta Libraries to reproduce single copies of this thesis and to lend or sell such copies for private, scholarly or scientific research purposes only. Where the thesis is converted to, or otherwise made available in digital form, the University of Alberta will advise potential users of the thesis of these terms.

The author reserves all other publication and other rights in association with the copyright in the thesis and, except as herein before provided, neither the thesis nor any substantial portion thereof may be printed or otherwise reproduced in any material form whatsoever without the author's prior written permission.

To my dearest family and friends
for their endless love and unconditional support

Acknowledgements

It has been a privilege to have both Prof. Biao Huang and Prof. Fraser Forbes as my supervisors. I consider them to be my idols, without whose continuous guidance and constructive criticism I would not have gained even the fraction of my achievements in University of Alberta. I appreciate all the help a I have got from the weekly meetings with Prof. Huang and Prof. Forbes, which was very important for each and every step of this research. They both took a lot of time to review and improve my work over and over. I am very grateful to their patience and encouragement during my two years' research work. Specially, the great opportunity of exploring industrial applications they have given me is greatly appreciated. Special thanks to Changbin Yu, for his long-lasting support and cooperation on our industrial project with Sherritt.

I am indebted to many people in the Computer Process Control Group for making my years in University of Alberta a priceless experience. First, I would like to thank Amir Alizadeh and Leily Mohammadi for sharing their knowledge of distributed parameter systems and experience in using simulation software. I would like to acknowledge Dr. Stevan Dubljevic for his instruction and advise about predictive control strategies for distributed parameter system. It was pleasant and memorable experience being able to work with the colleagues in CPC group. I would like thank Fei Qi, Yu Zhao, Ruben Gonzalez, Aditya Tulsyan, Li Xie, Lei Chen, Yijia Zhu, Da Zheng, Yu Yang, William Weng and every other group member. Wish you all the best in your future endeavor. Financial support from Natural Sciences and Engineering Research Council of Canada (NSERC) and technical support from Sherritt International Cooperation is greatly acknowledged.

Lastly, I would like to express my sincere appreciation and love to my family members. They always encouraged and supported me to follow my own dreams and for that I will be eternally grateful to them.

Abstract

In the steam methane reforming process, improvement of the reformed gas outlet temperature control performance can lead to a larger hydrogen production rate, while ensuring safe process operation. In this work, a side fired primary gas reformer is investigated. The three objectives of this work are: 1) to develop a process model that describes the dynamic relationship between the temperature of the reformed gas (process output) and the process variables consisting of manipulated and disturbance variables; 2) to develop optimization strategies for manipulating side-fired burners in order to provide smooth heat flux profiles that can prolong tube life and uniform reformed gas outlet temperatures; 3) to design predictive controllers that regulate the production process accurately.

As a first step, dynamic models for a generic primary gas reformer are developed by using homogeneous-phase one-dimensional reaction kinetics equations to describe the chemical reactions inside the reforming tubes and computing the external heat transfer to the tubes by radiation and convection. The model consists of a set of 1) coupled non-linear hyperbolic Partial Differential Equations (PDEs), which describe the product conversion rate and temperature profiles along each fixed bed catalytic tube reactors inside the furnace; 2) Ordinary Differential Equations (ODEs), which describe the temperatures of combustion gas and refractory walls; and 3) Algebraic Equations (AEs), which describe the heat flux profiles along the refractory walls towards tube reactors. These dynamic models lay a foundation for system optimization and optimal control design.

Mixed Integer Non-Linear Programming (MINLP) technique is used with the process model to determine optimal steady state operation condition. The objective is to find the optimal operating conditions for the side wall burners to maintain uniform reformed gas outlet temperatures within a certain range and to provide approximately flat profiles of radiant heat flux to the tubes. Four objective functions are proposed and their performances are compared. Constant disturbance effects that may cause uneven distribution in the system is also studied.

Model Predictive Control (MPC) application using both early-lumping (a conventional

MPC) and late-lumping (Characteristic-based MPC) approximations is studied for the outlet temperature control of the primary gas reformer. Set-point tracking and disturbance rejection performances of the two MPC controllers are evaluated. It is demonstrated that both predictive controllers are capable of providing satisfactory performance, while CBMPC yields a much shorter convergence time. Difference between the two controllers are further discussed.

Contents

1	Introduction	1
1.1	Motivation	2
1.2	Technical Background	3
1.2.1	Distributed Parameter System (DPS)	3
1.2.2	Mixed Integer Non-Linear Programming (MINLP)	5
1.2.3	Model Predictive Control (MPC)	7
1.2.4	Method of Characteristics	8
1.3	Scope of work	11
1.4	Contributions	13
2	Dynamic Modelling and Simulation of a Primary Gas Reformer	14
2.1	Gas Reforming Process Overview	14
2.2	Furnace Geometry of the Primary Reformer	16
2.3	Mass Balances	17
2.4	Heat Balances	20
2.4.1	Combustion Heat	21
2.4.2	Radiation Heat Flux	22
2.5	Momentum Balance	23
2.6	Development of Mathematical Models	24
2.6.1	Modelling Assumptions	25
2.6.2	Model Equations	25
2.6.3	Specifying Discretisation Methods for DPS	26
2.7	Steady State Simulation and Model Validation	28
2.8	Dynamic Simulation and Discussion	34
2.9	Conclusion	38
3	Optimization Strategies for Burner Operation	39
3.1	Problem Formulation	40
3.2	Optimization Studies using gPROMS	41
3.2.1	Solution Techniques	42
3.2.2	Error Analysis of Optimization Results	43

3.2.3	Comparison of Different Optimization Strategies	43
3.3	Disturbance Effects	46
3.4	Conclusion	47
4	Model Predictive Control (MPC) of Outlet Temperatures	48
4.1	Characteristic-Based Model Predictive Control	49
4.1.1	Set-point tracking	52
4.1.2	Regulatory behaviour	53
4.2	A Conventional MPC	54
4.2.1	Set-point tracking	62
4.2.2	Regulatory behaviour	63
4.3	Conclusion	65
5	Conclusions	68
5.1	Summary	68
5.2	Future Work	70
	Bibliography	70

List of Figures

1.1	The basic steps of Outer Approximation algorithm	6
1.2	States prediction along characteristic curves for scalar quasilinear hyperbolic PDE systems	11
2.1	Schematic of gas reforming process	15
2.2	Side and top view of the reforming furnace	16
2.3	Conventional diagram of side-fired primary reformer	17
2.4	Heat flux profile on a vertical section (Lengthwise) with all burners on . . .	23
2.5	Heat flux profile on a vertical section (Lengthwise) with burner(3,5) off . .	23
2.6	Tubes selected for model validation	28
2.7	Steady states profiles along a reforming tube(top to bottom)	28
2.8	Steady states profiles of outlet states at different s/c ratios	29
2.9	Steady states profiles of outlet states at different process gas flow rates . . .	30
2.10	Steady states profiles of outlet states at different fuel gas flow rates	31
2.11	Steady states profiles of outlet states at different ambient temperatures . .	32
2.12	Steady state validation (normalized)	33
2.13	Model response to a step change in the fuel gas flow rate	34
2.14	Model response to a step change in the process gas flow rate	35
2.15	Model response to a step change in the steam/carbon ratio	35
2.16	Model response to a step change in the ambient temperature	36
2.17	Outlet temperature profiles with side burners switched off I	37
2.18	Outlet temperature profiles with side burners switched off II	37
3.1	Process gas outlet temperatures from different burner operating strategies .	44
3.2	Ambient temperature profile along the refractory wall	46
3.3	Process gas outlet temperature before and after optimization with a constant disturbance	47
4.1	Set-point tracking response of CBMPC	52
4.2	Control signals of fuel gas flow rate and burner states	52
4.3	Disturbance rejection of CBMPC	53
4.4	Control signals of fuel gas flow rate and burner states	54

4.5	Flow chart of system identification	55
4.6	Tests of impulse response	57
4.7	Residual tests	58
4.8	Infinite-step prediction performance	59
4.9	Infinite-step prediction validation	60
4.10	The pole-zero map of the MISO system	61
4.11	Set-point tracking response of the conventional MPC	63
4.12	Control signals of fuel gas flow rate and burner states	63
4.13	Set-point tracking response of the conventional MPC	64
4.14	Control signals of fuel gas flow rate and burner states	64
4.15	Performance comparison of two predictive controllers in set-point tracking .	65
4.16	Performance comparison of two predictive controllers in disturbance rejection	66

List of Tables

2.1	Numerical methods for distributed systems in gPROMS	26
2.2	Model parameters for the industrial gas reformer	27
2.3	Process variables to different operating conditions of steam/carbon (s/c) ratio	30
2.4	Process variables to different operating conditions of process gas flow rate .	30
2.5	Process variables to different operating conditions of fuel gas flow rate . . .	31
2.6	Process variables to different operating conditions of ambient temperature .	32
2.7	Comparison between plant and simulated data (normalized)	33
3.1	Error analysis of optimization results	43
3.2	Comparison between optimization results	45

List of Symbols

- A_r Area of refractory wall(m^2)
- C_A Concentration of component A(mol/m^3)
- C_p Average specific heat of the process gas($kJ/molK$)
- C_{pg} Average specific heat of the furnace gas($kJ/molK$)
- d_i Tube inner diameter(m)
- d_o Tube outer diameter(m)
- D_{AZ} Diffusion coefficient(m^2/min)
- D_p Pellet equivalent diameter of the catalyst particle
- E_a Activation energy of a reaction(J/mol)
- F Mole flow rate of process gas(mol/min)
- F_g Mole flow rate of furnace gas(mol/min)
- ΔH Heat of reaction(kJ/mol)
- h_{comb} Heat of combustion(J/kg)
- K Absorption constant of a species
- K_{eq} Equilibrium constants for a reaction
- k Reaction rate of component A ($kmol/min/kgcat$)
- N_t Number of tubes in the furnace(mol/min)
- q Heat flux ($kJ/min/m^2$)
- q_r Radiation heat flux ($kJ/min/m^2$)
- r Reaction rate($kmol/min/kgcat$)
- T Temperature of the process gas(K)

T_w Temperature of the tube wall(K)
 T_g Temperature of the furnace gas(K)
 T_r Temperature of the refractory wall(K)
 u_l Velocity of the process gas through the tube reactor(m/min)
 ΔV Volume element(m^3)
 X Conversion rate
 y Mole fraction of a species
 z Distance from inlet of tube(m)
 ρ Process gas density(kg/m^3)
 ρ_g Furnace gas density(kg/m^3)
 ρ_B Catalyst bed density(kg/m^3)
 sc Mole feed ratios of steam and CH_4
 hc Mole feed ratios of H_2 and CH_4
 dc Mole feed ratios of CO_2 and CH_4
 nc Mole feed ratios of N_2 and CH_4
 x model state(s)
 u model input(s)
 i Reaction i
 in inlet
 out outlet
 $mean$ mean value
 t top value
 m medium value
 b bottom value

List of Symbols

- AE Algebraic Equation
- APC Advanced Process Control
- PDE Partial Differential Equation
- ODE Ordinary Differential Equation
- DAE Differential and Algebraic Equations
- DPS Distributed Parameter System
- LPS Lumped Parameter System
- PFR Plug-Flow Reactor
- MPC Model Predictive Control
- RHC Receding Horizon Control
- NMPC Non-linear Model Predictive Control
- FOPTD First Order Plus Time Delay
- MINLP Mixed Integer Non-linear Programming
- LQG Linear Quadratic Gaussian
- PID Proportional Integral Derivative
- SQP Sequential (or Successive) Quadratic Programming
- ARX AutoRegresive model with eXternal input
- ARMAX AutoRegressiveMoving-Average model with eXogenous inputs
 - BJ Box-Jenkins
 - OE Output-Error
- PEM Prediction Error Method

Chapter 1

Introduction

The gas reforming process is important in chemical industry, with application in several production schemes including hydrogen, ammonia and methanol. The process converts hydrocarbons (predominately methane) with steam to synthesis gas (H_2 , CO and CO_2) [45]. It has been used for years as the principal process for generating hydrogen and synthesis gas in chemical industry, with its popularity attributed to its higher efficiency and cost effectiveness when compared with other competing processes. Natural gas is commonly used as the feedstock of a gas reformer. Most production schemes stage the steam reforming across two reactors, primary and secondary reformers. For example, in the ammonia production process, the endothermic steam reforming reactions take place in the catalytic fixed-bed (tube) reactors within the primary reformer furnace, where the burners are installed on the refractory walls of the furnace in different arrangements. The reformed gas and preheated compressed air (supplies the nitrogen required for ammonia synthesis) enter into the secondary reformer so that combustion (supplying the heat required for reforming reactions) and reforming reactions simultaneously occur in the secondary reformer.

For different configurations of primary gas reformers, the burners can be located in different places of a furnace: on the roof (top-fired), on the floor (bottom-fired), or on the walls (side-fired or terrace-wall-fired). The flows of furnace gas and process gas can be either co-current or counter-current. The gas reformer studied in this work is side-fired and counter-current. The furnace gas enters through side-fired burners evenly distributed on both refractory walls, and after combustion, flows upward driven by the exhaust fan installed at the top of the furnace. The process gas enters at the top of the reformer and exits at the bottom, and flows through parallel rows of catalyst filled tubes. In the tubes, the hydrocarbons and steam react to form hydrogen, carbon dioxide and carbon monoxide. The reactions are catalysed by a nickel alloy catalyst and are predominantly endothermic. The heat needed to drive the endothermic reactions is provided by the combustion of fuel and radiation of the flames and refractory wall on the furnace side.

Since the reforming reactions are highly endothermic and require continuous heat supply, the reacting feedstock inside the tubes of the primary reformer will extract heat from the

tube wall, thus cooling the tube metal. The result is that process outlet temperatures are hundreds of degrees lower than the surrounding furnace temperature; however, if heat is applied non-uniformly, a side reaction may proceed to deposit carbonaceous polymers, known as coke, on the inside tube wall. Coke sticks to the tube walls and insulates the process fluid from the furnace. This can result in local overheating of the tube surface and ultimately, if neglected, tube ruptures. Therefore, keeping the heat provided to the tubes uniform will not only enhance the production rate, but also prolong tube service life.

In the steam methane reforming process, improvement of the reformed gas outlet temperature control performance can lead to a larger hydrogen production rate while ensuring the process operation safety. Many variables such as process/fuel gas inlet flow rate and burner status can affect the control objective. In this work, a side fired primary gas reformer is investigated. One major objective of this project is to develop a process model that describes the dynamic relationship between the temperature of the reformed gas (process output) and the process variables consisting of manipulated and disturbance variables.

1.1 Motivation

The work on this thesis was motivated by a request to develop a complete mathematical model of the gas reforming process, with a detailed investigation of the heat transfer mechanisms for a side-fired primary gas reformer. As world oil production decreases, natural gas (large reserves of which are still largely undiscovered) as an energy carrier will become more important, which increases the relevance of gas refining [45][44][63]. Gas reformers are of great interest to those plants with hydrogen or ammonia production units. New control and optimization strategies within reforming processes should therefore be developed to capture the possible material and energy savings [63].

The tubes in the primary reformer, made of metal alloys that experience creep at high temperatures and oxidizing environment with a designed life of 100,000 hours [22], are one of the most expensive components in the plant. Tube failures in primary reformers, resulting in costly tube replacements, plant shut downs and production losses [12], are attributed to creep rupture, stress rupture, bowing or hot bands. The causes of reformer tube failures include over firing, thermal shocks, steam condensation over the catalyst, and impact of thermal and pressure cycling from frequent start-ups and shut-downs [42]. The creep life is highly sensitive to temperature and pressure changes in the tubes, which may fluctuate significantly due to the changes in operating conditions and disturbances [12][7]. Therefore, monitoring tube temperature, maintaining a well-defined burner flame geometry and ensuring even flow through the tubes are vital aspects of reformer operations that can achieve a better tube service life.

Reliable dynamic models for industrial scale steam-methane fixed-bed reactors with sided-fired furnace heating type are still lacking. Therefore, the three objectives of this work are: 1) to develop a process model that describes the dynamic relationship between

the temperature of the reformed gas (process output) and the process variables consisting of manipulated and disturbance variables; 2) to develop optimization strategies for manipulating side-fired burners in order to provide smooth heat flux profiles that can prolong tube life and uniform reformed gas outlet temperatures; and 3) to design predictive controllers in order to regulate the production process accurately.

1.2 Technical Background

Many processes (e.g., tubular reactors and heat exchangers) in the field of chemical engineering are distributed parameter systems. The characteristics of the distributed parameter system (DPS) depend on the type of partial differential equations (PDEs) by which the system is described. Therefore, providing some background information of distributed parameter system and partial differential equations is of necessity. In addition, background for the method of characteristics approach, optimization techniques (such as mixed-integer non-linear programming and sequential quadratic programming) and an optimal control strategy (model predictive control) are also included in this section for introductory purposes.

1.2.1 Distributed Parameter System (DPS)

Arising from different areas of science and engineering, a great variety of systems are characterized by dependent variables (state variables) in two or more coordinates (independent variables). Time and space are the most frequent independent variables [65]. In the field of process engineering, DPS is a process in which the states, outputs and control variables may vary in space as well as in time. DPS is commonly modelled by a set of PDEs which stem from fundamental material, energy and momentum balances for a process, and include boundary conditions and initial conditions. When the process variables are spatially uniform or only the spatial average of process variables is of interest, the process can be considered to be Lumped Parameter System (LPS) [55], whose state variables are described by Ordinary Differential Equations (ODEs). It is not surprising to see in the industrial systems that DPS can interact with LPS as well as supplementary Algebraic Equations (AEs) for description of thermodynamic equilibria and etc. Before dynamic analysis and control design of such systems, it is often a prerequisite to establish a mathematical model to describe the chemical processes of the system. Such mathematical models commonly consist of a mixed set of non-linear PDEs, ODEs and AEs.

Taking time and space as the independent variables, an i^{th} order PDE for DPS are often of the following form:

$$F(t, z, x, \frac{\partial x}{\partial t}, \frac{\partial x}{\partial z}, \frac{\partial^2 x}{\partial t^2}, \frac{\partial^2 x}{\partial z^2}, \frac{\partial^2 x}{\partial t \partial z}, \dots, \frac{\partial^i x}{\partial z^i}, \frac{\partial^i x}{\partial t^i}, u) = 0 \quad (1.1)$$

where t and z are independent variables of time and space respectively, x is dependent variable of t and z , u is the manipulated variable. Note that the order of PDE is given by

its highest order partial derivative. Owing to a focus of this thesis on DPS, the classification of PDEs is explained here in more detail.

PDEs can be hyperbolic, parabolic or elliptic. Classification varies with different orders and linearity of PDEs. It is worth noting that **all first order PDEs are hyperbolic**. To understand more about characteristics of higher order PDEs, readers are referred to the reviews by Shang [55] and McOwen [41]. The PDEs considered in this work are first-order PDEs, which are usually classified as linear, quasilinear, or non-linear.

A first-order PDE is considered as linear [41] if it can be expressed in the form:

$$\frac{\partial x}{\partial t} + a(t, z, u) \frac{\partial x}{\partial z} + b(t, z, u)x = f(t, z, u) \quad (1.2)$$

The PDE is said to be quasilinear [55] [2] [13] [41] if it can be expressed in the form:

$$\frac{\partial x}{\partial t} + a(t, z, x, u) \frac{\partial x}{\partial z} = f(t, z, x, u) \quad (1.3)$$

The PDEs which are neither linear or quasilinear are said to be non-linear PDEs. In this study, the DPS consists of coupled first-order quasilinear hyperbolic PDEs with single characteristics.

Once a mathematical model for DPS is obtained, the next task is to develop a system simulation. The inherent complexity and non-linearity of the mathematical model may make the analytical solution intractable [65]. In the last decades, a vast number of numerical algorithms have been proposed for different types of PDEs (e.g. diffusion-reaction system, hyperbolic system, etc). One popular approach involves spatial approximation and time integration. More theoretical and practical aspects of the numerical approximation techniques for DPS can be found in [65].

The numerical approximation techniques for control purposes can be classified as:

- 1) **Early Lumping:** The PDEs are firstly approximated (lumped) by performing a spatial discretization, which derives a set of ODEs. The controller design proceeds with the lumped model equations (ODEs). With the application of the approximation technique, fundamental control theoretical properties (controllability, observability and stability) are lost [39] [8] [49]. This generally leads to high dimension controllers which are difficult to implement [8].
- 2) **Late Lumping:** The distributed nature of the system is kept as long as possible by late lumping approximation technique in the course of control design. In the end, numerical approximation techniques are still required to implement the resulting control algorithms. However, direct handling of PDEs is difficult and generally leads to a state feedback control law, which requires the design of an observer for practical implementation [39]. Successful applications of late lumping approximation for control design can be found in the work of Christofides [8] and Shang [26] [25]

1.2.2 Mixed Integer Non-Linear Programming (MINLP)

Mixed-Integer Non-linear Programming (MINLP) is an optimization approach to solve problems where both continuous and discrete decisions have to be made, and the objective function and/or feasible region of the problem are described by non-linear functions. In general, MINLP problems can be represented in the basic algebraic form as follows:

$$\underset{x,y}{\text{minimize}} \quad f(x,y) \quad (1.4)$$

subject to

$$g(x,y) = 0 \quad (1.5)$$

$$h(x,y) < 0 \quad (1.6)$$

$$x = (x_1, x_2, \dots, x_n) \in X, \text{ continuous variables}$$

$$y = (y_1, y_2, \dots, y_n) \in Y, \text{ integer variables.}$$

For the general case, the functions $f(x,y)$, $g(x,y)$ and $h(x,y)$ are non-linear. The decision variables x and y are continuous and discrete variables, respectively. X and Y are bounding-box-type restrictions on the variables. The continuous variables may be used to describe flow rates, concentration, volumes, and so forth. The integer variables (often binary variables) are discrete variables, and could describe the status of valves or pumps (i.e., on or off), equipment sizes or the topology of a process network.

The difficulty in solving MINLP problems is that they combine the difficulties inherent in the combinatorial nature of mixed integer programming (MIP) problems and the complexity of non-linear programming (NLP) problems. Methods for solving MINLPs include approaches and techniques extended from MIP, which rely on the successive solutions of closely related NLP problems. The most popular method for solving MINLP models are: Generalized Benders Decomposition (GBD), Branch and Bound (BB), Outer Approximation (OA), and Feasibility Approach (FA). In this work, we use the Outer Approximation (OA) method to solve the MINLP problem.

The Outer Approximation (OA) algorithm was first proposed by Duran and Grossmann [15] with linear constraints for integer decision variables and improved by Fletcher and Leyffer [20] with non-linear constraints for integer decision variables. Kocis and Grossmann [35] modified the OA algorithm for solving global optimization of the non-convex MINLP. The basic idea of the OA algorithm includes solving a MILP master problem and an alternating sequence of NLP subproblems [15] [14]. An initial system configuration is firstly specified, and by optimizing continuous variables with temporarily fixed integer variables, a solution for an NLP subproblem provides an upper bound on the cost of the MINLP problem [14]. The solution is then applied as a base point for MILP master problem which represents a linear approximation to MINLP at the continuous point. By adding linear outer-approximations, the continuous feasible region is overestimated and cost function is underestimated, which provides a lower bound on the solution of MINLP. If the upper

bound is greater than lower bound, the solution is feasible and is used as the initial configuration for the next iteration starting from solving NLP subproblems. The iteration can be stopped when no feasible solution is found (lower bound is greater than upper bound) and the processing structure is the optimal solution. Figure 1.1 illustrates the basic procedures of Outer Approximation algorithm.

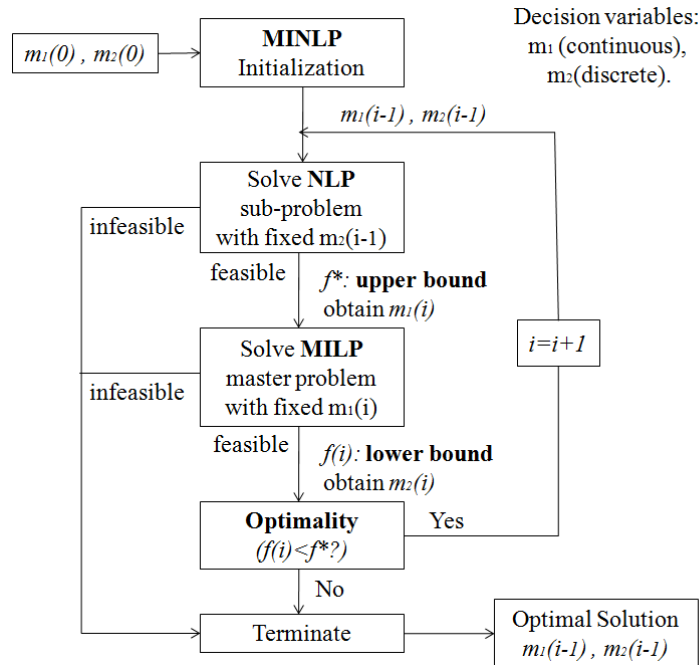


Figure 1.1: The basic steps of Outer Approximation algorithm

A large variety of methods have been proposed to solve constrained non-linear programming (NLP) problems (refer to comprehensive reviews on constrained non-linear optimization methods in [46] [52] [3] [21]). All of these methods use quadratic approximations to composite the objective function and equations of constraints [46] [23]. Sequential Quadratic Programming (SQP) method, one of the most popular algorithms for solving NLP, uses a quadratic approximation of the Lagrangian function as the objective function in the QP sub-problem with linear approximations of the constraints at the current point x_k , and applies the solution of sub-problem to calculate the next state x_{k+1} . The approximation procedure is done iteratively until a local minimum is reached. The basic idea of SQP is analogous to Newton method, which solves non-linear problems by successive solution of linear problems using a Taylor series expansion at each iterate. A more extensive and detailed coverage of the SQP method can be found for example in Wilson [64], Beale [4] and Fletcher [19].

1.2.3 Model Predictive Control (MPC)

Model Predictive Control (MPC), also known as Receding Horizon Control (RHC), has experienced tremendous growth in both research and industrial applications. As an advanced control method, MPC involves calculating future behaviour of the plant based on a process model, and solving an open-loop optimal control problem, subject to constraints. In this work, we will consider the implementation aspects of the non-linear model predictive control.

The system under consideration in this work will be represented by a set of non-linear differential (including ordinary and partial differential) and algebraic equations (DAE). Approximation methods such as finite difference and method of characteristics can be applied to convert the PDE system into ODEs to reduce the mathematical complexity arising from the PDEs. The mathematical formulation of the MPC problem for a system with dynamics that can be described by ODEs can be converted into the following discrete forms,

$$x_{t+1} = x_t + f(x_t, u_t)\Delta t \quad (1.7)$$

subject to the state and input constraints of the form:

$$x_t \in \mathcal{X}, \quad u_t \in \mathcal{U} \quad (1.8)$$

where $x_t \in \mathcal{R}_x^n$ are the state variables, and $u_t \in \mathcal{R}_u^n$ are the manipulated variables of the system. The feasible sets for input and states are denoted by \mathcal{X} and \mathcal{U} , defined by,

$$\mathcal{X} = \{x \in \mathcal{R}_x^n | x_{min} \leq x \leq x_{max}\} \quad (1.9)$$

$$\mathcal{U} = \{u \in \mathcal{R}_u^n | u_{min} \leq u \leq u_{max}\}. \quad (1.10)$$

The optimization problem $J \in \mathcal{R}$ is chosen to be quadratic and only contains state and input variables:

$$J = \min_u \left[\sum_{i=1}^{T_p} (\hat{x}_{t+i} - r_{t+i})^T Q(i) (\hat{x}_{t+i} - r_{t+i}) + \sum_{j=1}^{T_c} (u_{t+j} - u_{t+j-1})^T R(j) (u_{t+j} - u_{t+j-1}) \right] \quad (1.11)$$

where r is the reference signal/set-point, \hat{x} is the model prediction, u is the manipulated variable, Q and R are weighting matrices on system states and inputs. In literatures [53] [60], researchers have focused more on the lumped parameter systems than distributed parameter systems for Non-linear Model Predictive Control (NMPC). For the design of NMPC for distributed parameter systems, strategies of approximation techniques [61] are usually used in order to reduce the mathematical complexity arising from the partial differential equations.

The predictive control is a model-based feedback control, in which a plant model is used to predict the system behaviour at future time horizon, cost function is minimized to

calculate the optimal control sequence, and the optimization is repeated at each sampling interval. The MPC algorithm consists of four steps with a predefined objective function and constraints.

- At sample time k , predict the process states $x(k+i)$, $i = 1, 2, \dots, T_p$, given the initial values of past states $x(k)$ and past input $u(k)$.
- Calculate the set of future control signal $u(k+i)$, $i = 1, 2, \dots, T_c$ by optimizing the objective function subject to constraints.
- Obtain the optimal control sequence $u(k+i)$, $i = 1, 2, \dots, T_c$, and at sample time $k+1$ implement the optimal input signal $u(k+1)$.
- Repeat the algorithm with new process states for the next sampling time.

Based on the process states and input signal obtained at time $t = k$, future states are predicted along the prediction horizon T_p and the input sequence is calculated by optimizing the objective function subject to constraints. The optimization of objective function (cost minimization) is used to calculate the optimal input sequence along the control horizon T_c in order to make the system output follow a given setpoint trajectory. Usually less than or equal to prediction horizon T_p , the control horizon T_c is defined as how far into the future the input is moved, after which, the input signal is kept constant for the rest of the prediction horizon. The receding horizon approach is applied for the implementation of calculated optimal control sequence, meaning that only the first step of the control sequence is applied. For the next sampling time $t = k+1$, the future process states and optimal control sequence are recalculated using the same procedure.

1.2.4 Method of Characteristics

The method of characteristics is a differential geometric approach constructing integral surfaces of PDEs [55], which is fundamental for output prediction and optimal control design. Geometric control theory was developed to allow controller design for linear, quasilinear, non-linear low dimensional PDEs [55]. Feedback controllers for hyperbolic DPS were shown to be capable of achieving adequate performance (c.f. Hanczyc and Palazoglu [29], Shang et al. [26]). In the paper of Shang et al. [25], a novel MPC scheme is proposed for the control of a quasi-linear hyperbolic DPS based on the Method of Characteristics. The scheme was later applied to convection dominated parabolic systems [27].

For some systems represented by hyperbolic PDEs, the PDEs can be converted to equivalent ODEs along characteristic curves. Solutions of these ODEs along the characteristic curves can be transformed into solutions for the original PDEs. The first order hyperbolic

PDE that may approximate the gas reforming system can be generalized as:

$$\frac{\partial x}{\partial t} + a \frac{\partial x}{\partial z} = f(t, z, x, u) \quad (1.12)$$

$$y = g(x) \quad (1.13)$$

where t and z are independent variables of time and space, respectively; x are the distributed state variables varying with time and space; u is the manipulated variable; y is the controlled variable; $a(u)$ and $f(t, z, x, u)$ are continuous functions; $g(x)$ is an output function.

In the space with coordinates (t, z, x) , there exists a characteristic vector field $\zeta = [1, a(u), f(t, z, x, u)]$ in Equation (1.12), which defines the characteristic ODEs. The characteristic equation for the preceding quasi-linear PDE is represented as:

$$\begin{aligned} \dot{t} &= 1 \\ \dot{z} &= a(u) \\ \dot{x} &= f(t, z, x, u). \end{aligned} \quad (1.14)$$

As the above characteristic ODEs are non-linear, numerical integration methods may be required rather than analytical integration methods, to calculate a sampled future output from the current state variables at discrete spatial points by simultaneously integrating Equation (1.14) along each characteristic curve with known initial conditions t_0, z_0, x_0 . Then:

$$t = t_0 + \Delta t \quad (1.15)$$

$$z = \int_{t_0}^t a(u) d\tau = \phi_z(\Delta t, u) \quad (1.16)$$

$$x = \int_{t_0}^t f(t, z, x, u) d\tau = \phi_x(\Delta t, z_0, x_0, u) \quad (1.17)$$

The prediction is carried out with the assumption that current state variables x_0 at m spatial points $x_1, x_2, \dots, x_{m-1}, x_m$, and the continuous function representing axial velocity $a(u)$ is a constant u_l . Thus, the sampling time $t_s = \Delta t = L/(mu_l)$, and the next m sampling times at which the process states can be predicted are:

$$\begin{aligned} \Delta t_1 &= t_1 - t_0 = t_s \\ \Delta t_2 &= t_2 - t_0 = 2t_s \\ &\vdots \\ \Delta t_m &= t_m - t_0 = mt_s \end{aligned} \quad (1.18)$$

The prediction of the states $x_i, i = 1, 2, \dots, m$ by numerical integration of the characteristic ODEs is calculated at each prediction time instant $t_i = t_0 + it_s, i = 1, 2, \dots, m$ and for each spatial point $z_i = iL/m, i = 1, 2, \dots, m$ (at the inlet $z_0 = 0$, the boundary conditions

are represented as $x_0(t)$). Therefore, prediction of states at t_1 is:

$$\begin{aligned}
x_1(t_0 + t_s) &= x_0(t_0) + \int_{t_0}^{t_0+t_s} f(x_0(\tau), u(\tau))d\tau \\
x_2(t_0 + t_s) &= x_1(t_0) + \int_{t_0}^{t_0+t_s} f(x_1(\tau), u(\tau))d\tau \\
&\vdots \\
x_i(t_0 + t_s) &= x_{i-1}(t_0) + \int_{t_0}^{t_0+t_s} f(x_{i-1}(\tau), u(\tau))d\tau
\end{aligned} \tag{1.19}$$

where $i = 1, 2, \dots, m$. With a well-chosen number of discrete points for process states prediction, the decoupling property allows prediction of the future states with relatively high accuracy without a high computational requirement. For the prediction of outlet states x_m at a particular prediction instant $t_i = t_0 + it_s, i = 1, 2, \dots, m$,

$$\begin{aligned}
x_m(t_0 + t_s) &= x_{m-1}(t_0) + \int_{t_0}^{t_0+t_s} f(x_{m-1}(\tau), u(\tau))d\tau \\
x_m(t_0 + 2t_s) &= x_{m-2}(t_0) + \int_{t_0}^{t_0+t_s} f(x_{m-2}(\tau), u(\tau)) + \int_{t_0+t_s}^{t_0+2t_s} f(x_{m-1}(\tau), u(\tau))d\tau \\
&\vdots \\
x_m(t_0 + i\Delta t) &= x_{m-i}(t_0) + \sum_{j=1}^i \int_{t_0+(j-1)t_s}^{t_0+jt_s} f(x_{m-j}(\tau), u(\tau))d\tau
\end{aligned} \tag{1.20}$$

As shown in Figure 1.2, the future states for the next t_p sample instants are calculated by integrating characteristic ODEs with initial values $x_m(t_0), x_{m-1}(t_0), \dots, x_1(t_0)$.

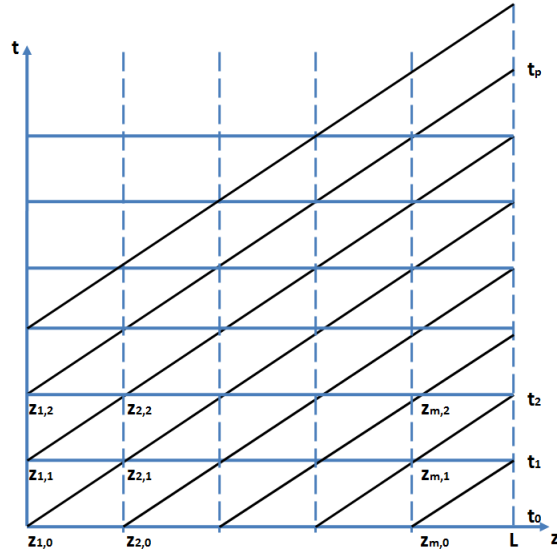


Figure 1.2: States prediction along characteristic curves for scalar quasilinear hyperbolic PDE systems

1.3 Scope of work

The main focus in this work is the development of a dynamic mathematical model for a side-fired primary gas reformer. The second major part of the thesis is the development of optimization strategies for manipulating side-fired burners in order to provide smooth heat flux profiles that can prolong tube life and uniform synthesis gas outlet temperatures. Finally, two model predictive controllers are designed using two different approximation techniques for prediction models in order to regulate the production process by controlling outlet temperatures.

In Chapter 2, an overview of the gas reforming process is provided. The dynamic mathematical model of a primary gas reformer, consisting of partial differential equations (PDEs) coupled with ordinary differential equations (ODEs) and algebraic equations, is developed. The steady state and dynamic modelling of a primary gas reformer are performed considering simultaneous radiation and convection heat transfer processes and chemical reforming reactions in the presence of catalyst. Numerical model simulations are validated using measured data recorded from an ammonia plant. The dynamic model lays a foundation for system optimization and optimal control design.

In Chapter 3, a mixed-integer non-linear programming (MINLP) based optimisation approach is developed for the gas reforming process using gPROMS [47] model builder. This chapter focuses on the development of steady state optimization strategies to manipulate side-fired burners, which are only available for manual operations. The dynamic process model is first computed with predetermined initial conditions until it reaches a stable steady states. A MINLP based optimisation solver, using the outer approximation algorithm, is

implemented for steady state optimization. Four objective functions focusing on the uniformity of synthesis gas temperatures from different tube reactors are proposed and simulations are carried out for different optimization purposes. The steady state optimization results serve as guidance for burner operations for some plants.

In Chapter 4, the non-linear predictive control problem is formulated and solved for a side-fired primary gas reformer. The objective of the MPC controller design is to manipulate fuel gas flow rate and burner states aiming at controlling the reformed gas outlet temperature with smaller fluctuations upon ambient temperature changes. Two different approaches to constructing the prediction model in the MPC controller are introduced, using early lumping (using an empirical model) and late lumping (using the full model and the method of characteristics) approximation techniques respectively. Simulation results of the two MPC controllers are compared for tracking and regulating behaviours. The performance of the Characteristic-Based Model Predictive Controller (CBMPC) is compared with lumped predictive controller in terms of computational load and control accuracy.

1.4 Contributions

The contributions of this thesis are summarized as follows:

- A dynamic mathematical model of gas reforming processes in primary gas reformers is developed. The reaction kinetics and heat transfer mechanisms involved in a side-fired primary gas reformer are investigated to provide detailed description of the dynamic relationship between the synthesis gas outlet temperatures and the process variables consisting of manipulated and disturbance variables.
- A mixed-integer non-linear programming (MINLP) based optimisation method is developed, with a focus on improving the uniformity of synthesis gas temperatures from different tube reactors by the manipulation of manually-operated side-fired burners. The steady state optimization results may serve as a guidance for burner operations.
- Two model predictive controllers are designed based on two different approximation approaches applied in the prediction models. Performance of the two MPC controllers are evaluated and compared with respect to their computational load and control accuracy.

Chapter 2

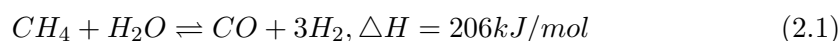
Dynamic Modelling and Simulation of a Primary Gas Reformer

The objective of this chapter is to develop a dynamic mathematical model for the gas reforming process in a side-fired primary gas reformer, taking into consideration the chemical kinetics along with the mass and heat transfer. Dynamic behaviour is simulated to study the performance of a primary reformer unit in an ammonia plant.

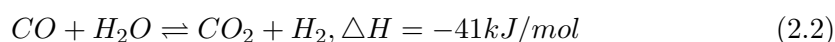
2.1 Gas Reforming Process Overview

Gas reforming, as a key and economic chemical reaction process, has been applied in industrial production schemes such as hydrogen, synthesis gas, methanol and ammonia. Due to the complex and varying chemical composition of the feedstock, multitude of chemical reactions take place in the gas reforming process and it seems impractical to account for all of the chemical reactions [18]. Xu et al. [66] considered a large number of detailed reaction mechanisms of gas reforming process using thermodynamic analysis and concluded three most important reversible reaction kinetics as follows:

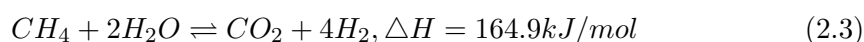
- Methane and Steam Reforming



- Water Gas Shifting



- Reverse Methanation



Reactions as shown in (2.1) and (2.3) are reversible and normally reach equilibrium over an active catalyst, at high temperatures. CO_2 is not only produced through the Water Gas

Shift(WGS) Reaction shown in (2.2), but also directly through the gas reforming reaction shown in (2.3). In fact Reaction in (2.3) results from the combination of reaction in (2.1) and (2.2). Because of the endothermic behaviour of gas reforming, a high temperature is favoured. The overall product gas (synthesis gas) is a mixture of carbon monoxide, carbon dioxide, hydrogen, and unconverted methane and steam. The temperature of the reactor, the operating pressure, the composition of the feed gas, and the proportion of steam fed to the reactor govern the exit concentrate of mixture from the reformer.

The gas reforming process consists of the following two steps [44]:

- The first step of the gas reforming process involves methane reacting with steam at 750-800°C (1380-1470°F) to produce a synthesis gas, a mixture primarily made up of hydrogen and carbon monoxide. The primary and secondary reformers are designed for this important reforming stage to provide external heat that is required for the reactions.
- In the second step, known as a water gas shift (WGS) reaction, the carbon monoxide produced in the first reaction is reacted with steam over a catalyst to form hydrogen and carbon dioxide. The process occurs in two stages, consisting of a high temperature shift (HTS) at 350°C (662°F) and a low temperature shift (LTS) at 190-210°C (374-410°F).

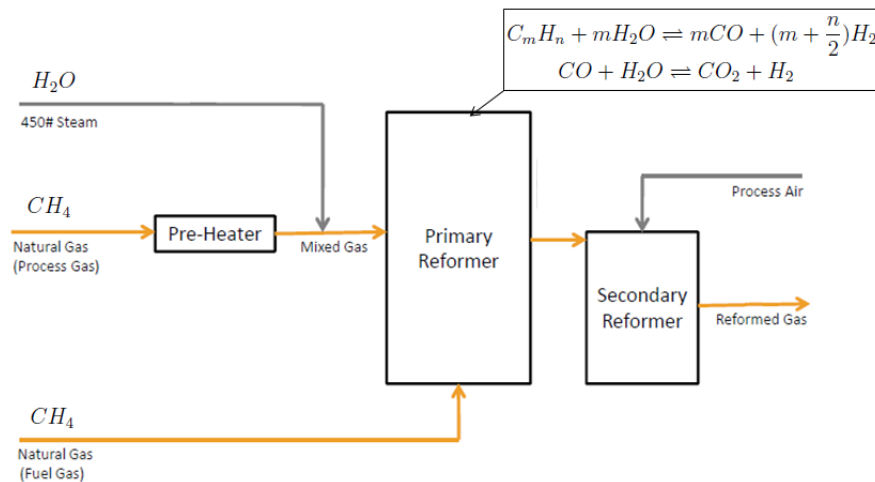


Figure 2.1: Schematic of gas reforming process

Figure 2.1 is a schematic of an industrial gas reforming process consisting of both primary and secondary reformers. The focus of this thesis is on primary gas reformer, where most of endothermic gas reforming reactions take place.

As the gas reforming process is a relatively mature technology, different types of steady state mathematical models that are used for simulations of the primary gas reformer have

been proposed in the literature; see, for example, the literature summary of Latham [36]. In this work, dynamic mathematical models based on mass and heat balances are considered.

2.2 Furnace Geometry of the Primary Reformer

For different configurations of primary gas reformers, the burners could be located in different places: on the roof (top-fired), on the floor (bottom-fired), or on the walls (side-fired or terrace-wall-fired). In this study, side-fired reformer is investigated, which means that the burners are located on the side walls. The furnace in this study is a side-fired furnace, and the side view and top view of the reforming furnace is shown in Figure 2.2.

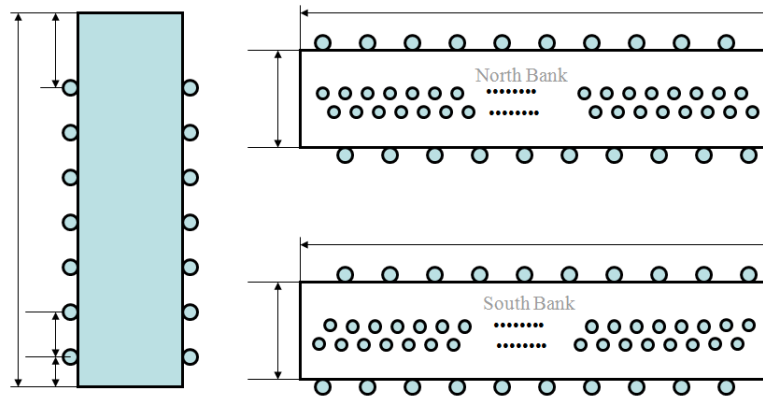


Figure 2.2: Side and top view of the reforming furnace

The gas reforming process considered in this work consists of hundreds of fixed bed tubular reactors combined with a heating furnace, which consists of two symmetric bands with 70 side burners evenly distributed along each wall; each band comprises 2 rows of 34 tubes of 10.36 m in length.

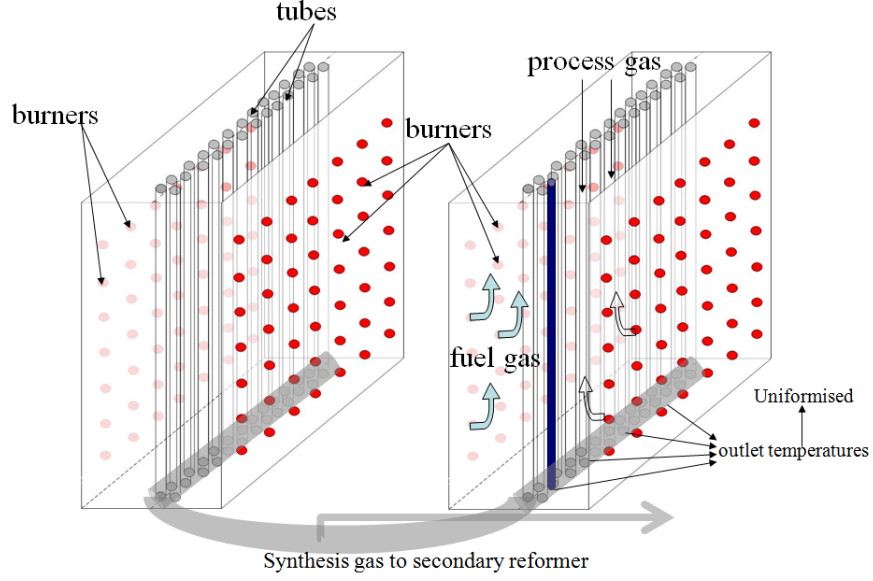


Figure 2.3: Conventional diagram of side-fired primary reformer

As shown in Figure 2.3, the fuel gas goes through burners into the furnace, and is collected at the top of furnace after combustion, driven by the fan installed above the furnace. The preheated process gas goes from the top of each tube to its bottom, and is collected through one tube as the feed into secondary reformer. In real plants there are several measurements for outlet temperatures in specific locations. The current strategy for controlling the process is to manually operate the burners to maintain a low standard deviation of the measured temperature values.

2.3 Mass Balances

The stoichiometry of the gas reforming process was introduced in Equations (2.1) - (2.3). Considering a tubular reactor in which n chemical reactions take place and the change the concentration of component A as the fluid moves down the tube, we use the following equations (Equations (2.4) to (2.6) [5]) to describe the mass balance of reactant component A in a volume element ΔV during a time interval Δt .

$$\begin{aligned} \Delta V C_A|_{t+\Delta t} - \Delta V C_A|_t = & \int_t^{t+\Delta t} [(FC_A|_V - D_{AZ} \frac{dC_A}{dz}|_V) \\ & - (FC_A|_{V+\Delta V} - D_{AZ} \frac{dC_A}{dz}|_{V+\Delta V}) - \rho_B k C_A \Delta V] dt \end{aligned} \quad (2.4)$$

where F is the volume flow rate, D_{AZ} is the diffusion coefficient, ρ_B is the density of the catalyst, and k is the reaction rate of component A.

Using the mean value theorem of integral calculus and dividing (2.4) by Δt and ΔV ,

we derive:

$$\frac{(C_A|_{t+\Delta t} - C_A|_t)}{\Delta t} = \frac{F(C_A|_V - C_A|_{V+\Delta V})}{\Delta V} + \frac{D_{AZ}(\frac{dC_A}{dz}|_{V+\Delta V} - \frac{dC_A}{dz}|_V)}{\Delta V} - \rho_B k C_A. \quad (2.5)$$

Letting Δt and ΔV go to zero yields:

$$\frac{\partial C_A}{\partial t} = -\frac{\partial F C_A}{\partial V} + \frac{\partial D_{AZ} \frac{\partial C_A}{\partial z}}{\partial V} - \rho_B k C_A. \quad (2.6)$$

For tube reactors with constant cross-sectional area, $dV = Adz$, $F = Au_l$, where u_l is the velocity along z direction. Thus, (2.6) can be written in the following PDE form:

$$\frac{\partial C_A}{\partial t} = -u_l \frac{\partial C_A}{\partial z} + D_{AZ} \frac{\partial^2 C_A}{\partial z^2} - \rho_B k C_A. \quad (2.7)$$

To solve this problem, the initial condition (concentration as a function of distance at the initial time) and one boundary condition must be given. Such as, $C_A(z, t = 0) = C_{A0}(z)$; $C_A(0, t) = C_{A,in}(t)$.

As the tube length/tube diameter ratio and tube length/particle diameter ratio for the gas reforming tube reactor are large (> 100), the back-mixing of the flow in the gas reforming tube reactor can be neglected [31]. At Reynolds numbers of 10^3 to 10^4 , as usually seen in gas reformers [51], the effect of diffusion is negligible compared to the bulk flow. Therefore, the diffusion term $D_{AZ} \frac{\partial^2 C_A}{\partial z^2}$ will not be considered in this work.

For systems with the existence of more than one reaction, the reaction term $\rho_B k C_A$ in Equation 2.7 should be expanded. Considering the temperature dependency of mole concentration characteristics, mole fraction is chosen to replace concentration for displaying the conversion effects of CH_4 and CO_2 :

$$\frac{\partial y_{CH_4}}{\partial t} = -u_l \frac{\partial y_{CH_4}}{\partial z} + \rho_B (n_1(z)r_1(z) + n_3(z)r_3(z)) \quad (2.8)$$

$$\frac{\partial y_{CO_2}}{\partial t} = -u_l \frac{\partial y_{CO_2}}{\partial z} + \rho_B (n_2(z)r_2(z) + n_3(z)r_3(z)) \quad (2.9)$$

$$y_{CH_4}(z = 0, t) = y_{CH_4,in}(t), \quad y_{CO_2}(z = 0, t) = y_{CO_2,in}(t)$$

where $n_1(z), n_2(z), n_3(z)$ are the effectiveness factors for reactions (2.1), (2.2) and (2.3) (see details in reference [18]); $r_1(z), r_2(z), r_3(z)$ are the rates of reactions (2.1), (2.2) and (2.3) with detailed expressions as follows:

$$r_1 = \frac{a_1 \exp(-E_{a_1}/RT)}{E^2 y_{H_2}^{2.5} P^{0.5}} \left(y_{CH_4} y_{H_2O} - \frac{P^2 y_{H_2}^3 y_{CO}}{K_{eq1}} \right) \quad (2.10)$$

$$r_2 = \frac{a_2 \exp(-E_{a_2}/RT)}{E^2 y_{H_2}} \left(y_{CO} y_{H_2O} - \frac{y_{H_2} y_{CO_2}}{K_{eq2}} \right) \quad (2.11)$$

$$r_3 = \frac{a_3 \exp(-E_{a_3}/RT)}{E^2 y_{H_2}^{3.5} P^{0.5}} \left(y_{CH_4} y_{H_2O}^2 - \frac{P^2 y_{H_2}^4 y_{CO_2}}{K_{eq3}} \right) \quad (2.12)$$

whereas

$$E = 1 + P(K_{CO}y_{CO} + K_{CH_4}y_{CH_4} + K_{H_2}y_{H_2}) + K_{H_2O} \frac{y_{H_2O}}{y_{H_2}} \quad (2.13)$$

where the adsorption constants K_{CO} , K_{CH_4} , K_{H_2} and K_{H_2O} are assessed by calculating the masses of components that are adsorbed on the catalyst of nickel, take the following expressions [18]:

$$K_{CH_4} = 6.65 \times 10^{-6} \exp\left(\frac{4604.28}{T}\right); kPa^{-1} \quad (2.14)$$

$$K_{H_2} = 6.12 \times 10^{-11} \exp\left(\frac{9971.13}{T}\right); kPa^{-1} \quad (2.15)$$

$$K_{CO} = 8.23 \times 10^{-7} \exp\left(\frac{8497.71}{T}\right); kPa^{-1} \quad (2.16)$$

$$K_{H_2O} = 1.77 \times 10^3 \exp\left(\frac{-10666.35}{T}\right); \text{unitless} \quad (2.17)$$

In the feedstock, it may also be found low levels of contaminants such as nitrogen, carbon dioxide, water and sulfur compounds [58]. According to Lim Yueh Yang et al. [18], *sc*, *hc*, *dc* and *nc* denote the mole feed ratios of *steam/CH₄*, *H₂/CH₄*, *CO₂/CH₄* and *N₂/CH₄*, and mole fractions for all the species are calculated as:

$$y_{CH_4} = \frac{1 - X_{CH_4}}{R + 2X_{CH_4}} \quad (2.18)$$

$$y_{CO_2} = \frac{dc + X_{CO_2}}{R + 2X_{CH_4}} \quad (2.19)$$

$$y_{H_2} = \frac{hc + 3X_{CH_4} + X_{CO_2}}{R + 2X_{CH_4}} \quad (2.20)$$

$$y_{CO} = \frac{X_{CH_4} - X_{CO_2}}{R + 2X_{CH_4}} \quad (2.21)$$

$$y_{H_2O} = \frac{sc - X_{CH_4} - X_{CO_2}}{R + 2X_{CH_4}} \quad (2.22)$$

whereas

$$R = 1 + sc + hc + dc + nc \quad (2.23)$$

2.4 Heat Balances

Tube Side

Similarly to the aforementioned strategy, the heat balance of the fluid in a volume element ΔV of a tubular reactor at a time interval Δt is described in Equations (2.24) to (2.29).

$$\Delta V \rho C_p (T|_{t+\Delta t} - T|_t) = \int_t^{t+\Delta t} \left\{ \rho C_p [(FT)|_V - D_{AZ} \frac{dT}{dz}|_V] - (FT)|_{V+\Delta V} - D_{AZ} \frac{dT}{dz}|_{V+\Delta V} \right\} - \rho_b \Sigma_1^n (r_i \Delta H_i) \Delta V + (\pi d_i \Delta h) h_{w1} (T_w - T) \} dt \quad (2.24)$$

Using the mean value theorem of integral calculus and dividing (2.24) by Δt and ΔV , we derive:

$$\frac{(T|_{t+\Delta t} - T|_t)}{\Delta t} = \frac{F(T|_V - T|_{V+\Delta V})}{\Delta V} + \frac{D_{AZ}(\frac{dT}{dz}|_{V+\Delta V} - \frac{dT}{dz}|_V)}{\Delta V} - \frac{\rho_b \Sigma_1^n (r_i \Delta H_i)}{\rho C_p} + \frac{(\pi d_i \Delta h) h_{w1} (T_w - T)}{\rho C_p \Delta V} \quad (2.25)$$

whereas

$$\Delta V = \frac{\pi d_i^2}{4} \Delta h \quad (2.26)$$

Letting Δt and ΔV go to zero yields:

$$\frac{\partial T}{\partial t} = -\frac{\partial FT}{\partial V} + \frac{\partial D_{AZ} \frac{\partial T}{\partial z}}{\partial V} - \frac{\rho_b \Sigma_1^n (r_i \Delta H_i)}{\rho C_p} + \frac{4h_{w1}(T_w - T)}{\rho C_p d_i} \quad (2.27)$$

For tube reactors with constant cross-sectional area, $dV = Adz$, $F = Au_l$, where u_l is the velocity along z direction. Thus, (2.27) can be written in the following PDE form:

$$\frac{\partial T}{\partial t} = -u_l \frac{\partial T}{\partial z} + D_{AZ} \frac{\partial^2 T}{\partial z^2} - \frac{\rho_b \Sigma_1^n (r_i \Delta H_i)}{\rho C_p} + \frac{4h_{w1}(T_w - T)}{\rho C_p d_i}. \quad (2.28)$$

To solve this problem, the initial condition (concentration as a function of distance at the initial time) and one boundary condition must be given. Such as, $T(z, t = 0) = T_0(z)$; $T(0, t) = T_{in}(t)$. Therefore, the PDE of temperature derived from heat balance (with no back-mixing) is

$$\frac{\partial T}{\partial t} = -u_l \frac{\partial T}{\partial z} + \frac{\rho_b \Sigma_1^n (r_i \Delta H_i)}{\rho C_p} + \frac{4h_{w1}(T_w - T)}{\rho C_p d_i} \quad (2.29)$$

From Equation (2.29), it is worth noting that, the dynamics of fluid temperature in a tubular reactor is not only correlated with chemical reactions, but also with the heat flux transferred into the reactor through the reactor wall.

Furnace Side

Since the reforming reactions are highly endothermic and require a continuous heat supply, the reacting feedstock inside the tube will extract heat from the tube wall, thus cooling the tube metal. The result is that process outlet temperatures are hundreds of degrees lower than the surrounding furnace temperature; however, if heat is applied non-uniformly, a side reaction may proceed to deposit carbonaceous polymers on the inside tube wall, known as coke. Coke sticks to the tube walls and insulates the process fluid from the furnace, which can result in local overheating of the tube surface and ultimately; if neglected, tube ruptures [11]. Therefore, keeping the heat provided to the tubes uniform will not only enhance the production rate, but also prolong tube service life.

The furnace side model considers heat transfer into the tubes and heat loss out of the furnace based on conservation of energy in the furnace. Heat transfer within the furnace mainly includes: radiation heat transfer from combustion flame to reforming tube walls, convective heat transfer from furnace wall to furnace gas and from furnace gas to reforming tube walls, and convective heat transfer from furnace wall to the air outside furnace. For the side fired furnace, it is assumed that the combustion gas is well mixed inside the furnace and its temperature is uniform. For the side fired reformer, the radiation heat from flames and furnace refractory walls has much more contribution than convection. The following equations represent heat balance of furnace gas.

$$\rho_g C_{pg} V \frac{\partial T_g}{\partial t} = F_g \rho_g h_{comb} - N_t \pi d_o \int_0^L h_{w2} (T_g - T_w(z)) dz - A_{ri} h_{w3} (T_g - T_r) \quad (2.30)$$

$$\begin{aligned} \rho_r C_{pr} V_r \frac{\partial T_r}{\partial t} = & A_{ri} h_{w3} (T_g - T_r) - A_{ro} h_{w5} (T_r - T_{amb}) \\ & + N_b A_b \sigma \varepsilon_f T_f^4 - A_{ri} \sigma \varepsilon_r T_r^4 - N_t \int_0^L \sigma \varepsilon_w T_w(z)^4 \end{aligned} \quad (2.31)$$

where ρ_g and ρ_r are densities of furnace gas and the refractory wall respectively; T_g , T_r , T_f , T_{amb} and T_w are process gas, refractory wall, flame and ambient temperatures respectively; h_{w2} and h_{w3} are convective heat transfer coefficients for fuel gas-tube wall and fuel gas-refractory wall respectively. h_{comb} is the heat of combustion as described in the following section.

2.4.1 Combustion Heat

The heat generated from the combustion of fuel gas in the furnace is represented as $F_g \rho_g h_{comb}$, where h_{comb} is called heat of combustion. Alhaddad et al. [1] modelled a Helmholtz pulse combustor by solving the conservation equations of mass, energy, and species, and the equation of state of an ideal gas. An adiabatic flame temperature can be estimated from the equivalence ratio for a given fuel. From tables of gas properties [16], a linear relationship between the heat of combustion and flame temperature can be established, especially within

a typical range of adiabatic flame temperature.

$$h_{comb} = aT_f + b \quad (2.32)$$

The values of coefficients a and b , for example, for air, are $1.2kJ/kg.K$ and $-159kJ/kg$, respectively, in the range of temperature $T_f = 800 - 2200K$. Note that a is an average value of the specific heat at constant pressure. In practice, these coefficients would vary with the equivalence ratio and fuel type, being established from the composition of products resulting from complete combustion and excess air. Since the model is built based on the assumption of constant source of fuel and complete combustion, with given specific flame temperature and the above assumptions, the value of heat of combustion for methane is selected to be $5 \times 10^7 J/kg$.

2.4.2 Radiation Heat Flux

The distribution of heat flux (the fraction of radiation incident to a tube at a given elevation), in which radiation accounts for a great proportion, is an important criterion for the performance of gas reforming units. For the side-fired gas reformer furnace, radiation heat is released instantly and short flame lengths are presumed so that the radiation can be treated as a point source. The overall heat received by one tube at a given elevation z , is given by

$$q(x, z) = h_{w1}(T_w(z) - T(z)) = \frac{d_o}{d_i} [q_r(x, z) + h_{w2}(T_g - T_w(z))] \quad (2.33)$$

where $q(x, z)$ is the heat flux from tube to process gas and h_{w1} is convective heat transfer coefficient between tube wall and process gas, while $q_r(x, z)$ is the radiation heat flux at point (x, z) , on the surface of which the burners are located, and is given as below:

$$q_r(x, z) = y_r(x, z)(\sigma\varepsilon_f T_f^4 - \sigma\varepsilon_r T_r^4) + \sigma\varepsilon_r T_r^4 \quad (2.34)$$

$$y_r(x, z) = \frac{1}{Y_{max}} \sum_{j=1}^{10} \sum_{i=1}^7 \frac{burner(i, j)\varpi}{\sqrt{\varpi^2 + (x - x_i)^2 + (z - z_j)^2}} \quad (2.35)$$

where $y_r(x, z)$ is the normalized coefficient of the combination of heat flux contributed from all the burners (7×10) which are switched on, and Y_{max} is the maximum heat flux value, ϖ is the width/height(inverse aspect ratio) of the furnace, and $burner(i, j)$ is the burner state(if burner is on, $burner(i, j) = 1$; if burner is off, $burner(i, j) = 0$).

Figure 2.4 and 2.5 present the two dimensional heat flux profiles by characterising normalized heat flux coefficients. Figure 2.4 illustrates heat flux profile with all side burners on, and Figure 2.5 illustrates heat flux profile with some burners off.

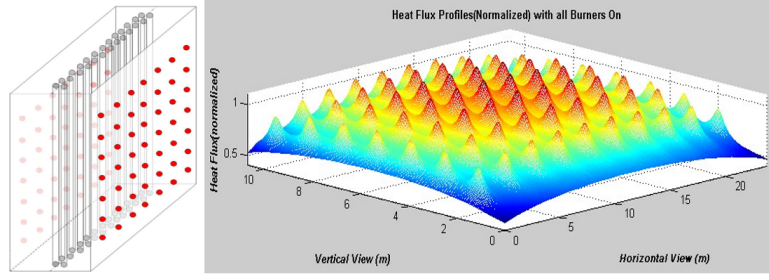


Figure 2.4: Heat flux profile on a vertical section (Lengthwise) with all burners on

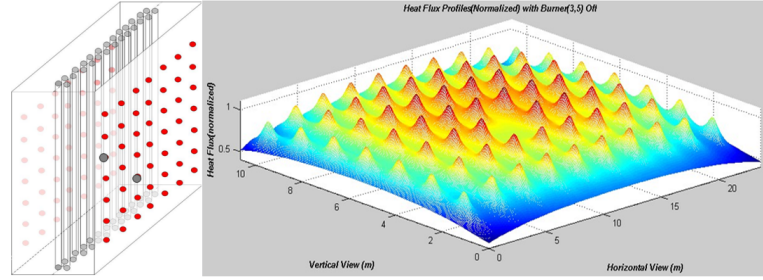


Figure 2.5: Heat flux profile on a vertical section (Lengthwise) with burner(3,5) off

2.5 Momentum Balance

According to Ergun [17], the pressure drop for a packed bed reactor, can be evaluated in turbulent flow regime by the following equation:

$$\frac{dP}{dz} = -\frac{1.75\rho_g u_t(1-v)}{\psi D_p(v)^3} \quad (2.36)$$

where ψ is the pellet sphericity, D_p is the pellet equivalent diameter of the catalyst particle and v is the catalyst bed void fraction.

Kehoe [34] came to the conclusion that pressure gradients have no significant effect on the pore diffusion, meaning that the momentum balance can be ignored in the pellet model. Burghardt and Aerts [6] drew the conclusion that the pressure changes are probably so small under normal industrial conditions that they can be neglected in reactor models, after evaluating the internal pressure change in a pellet with reaction and mass transfer by Knudsen diffusion, molecular diffusion and viscous convective flow. Similar results can also be found in the work of Veldsink [62] and Nan [43]. The conclusions summarized above are brought forward to a simplified version with a known inlet pressure and constant pressure drop in the tube reactor model of this thesis.

2.6 Development of Mathematical Models

The gas reforming process considered in this work consists of typically hundreds of fixed bed tubular reactors vertically installed in a side-fired heating furnace. A single dynamic tubular reactor is described as a dynamic pseudo-homogeneous model using partial differential equations (PDEs) developed from mass and heat balance (see details from Section 2.2).

$$\frac{\partial y_{cH_4}}{\partial t} + u_l \frac{\partial y_{cH_4}}{\partial z} = \rho_B (n_1(z)r_1(z) + n_3(z)r_3(z)) \quad (2.37)$$

$$\frac{\partial y_{cO_2}}{\partial t} + u_l \frac{\partial y_{cO_2}}{\partial z} = \rho_B (n_2(z)r_2(z) + n_3(z)r_3(z)) \quad (2.38)$$

$$\frac{\partial T}{\partial t} + u_l \frac{\partial T}{\partial z} = -\frac{\rho_b}{\rho C_p} \left(\sum_{i=1}^3 (r_i(z)\Delta H_i) \right) + \frac{4h_{w1}(T_w - T)}{\rho C_p d_i} \quad (2.39)$$

$$\frac{\partial T_w}{\partial t} + u_l \frac{\partial T_w}{\partial z} = \frac{4d_o h_{w2}(T_g - T_w) - 4d_i h_{w1}(T_w - T) + 4d_i (q_r - \sigma \varepsilon T_w^4)}{\rho_t C_{pt} (d_o^2 - d_i^2)} \quad (2.40)$$

$$\begin{aligned} \frac{\partial T_g}{\partial t} &= \frac{F_g \rho_g h_{comb}}{\rho_g C_{pg} V} \\ &- \frac{N_t \pi d_o \int_0^L h_{w2}(T_g - T_w(z)) dz - A_{ri} h_{w3}(T_g - T_r)}{\rho_g C_{pg} V} \end{aligned} \quad (2.41)$$

$$\begin{aligned} \frac{\partial T_r}{\partial t} &= \frac{A_{ri} h_{w3}(T_g - T_r) - A_{ro} h_{w5}(T_r - T_{amb})}{\rho_r C_{pr} V_r} \\ &+ \frac{\sigma (N_b A_b \varepsilon_f T_f^4 - A_{ri} \varepsilon_r T_r^4 - N_t \int_0^L \varepsilon_w T_w^4)}{\rho_r C_{pr} V_r} \end{aligned} \quad (2.42)$$

The boundary and initial conditions are:

$$y_{cH_4}(z = 0, t) = y_{cH_4,in}(t), \quad (2.43)$$

$$y_{cO_2}(z = 0, t) = y_{cO_2,in}(t), \quad (2.44)$$

$$T(z = 0, t) = T_{in}, \quad (2.45)$$

$$T_w(z = 0, t) = T_{w,in}, \quad (2.46)$$

$$y_{cH_4}(t = 0) = y_{cH_4,in}(0), \quad (2.47)$$

$$y_{cO_2}(t = 0) = y_{cO_2,in}(0), \quad (2.48)$$

$$T(t = 0) = T_{in}(0), \quad (2.49)$$

$$T_w(t = 0) = T_{w,in}(0), \quad (2.50)$$

$$T_g(t = 0) = T_{g,in}(0), \quad (2.51)$$

$$T_r(t = 0) = T_{r,in}(0) \quad (2.52)$$

2.6.1 Modelling Assumptions

The models are built based on the following assumptions:

- The reformed gas (process gas) flows with complete radial but no axial mixing.
- The combustion gas (fuel gas) is well mixed.
- The radiation heat transfer between tubes is neglected.
- The radial temperature profiles of reforming tubes are neglected, but the axial temperature changes are considered.

2.6.2 Model Equations

As aforementioned assumptions and discussions, the mathematical model of steam methane reforming process involves a set of coupled PDEs and ODEs. On the basis that diffusion is small in comparison to convection, the diffusion term can be omitted, and the distributed parameter system is stated by a set of hyperbolic PDEs. Then the original dynamic model, Equations (2.37) - (2.42), can be simplified to:

$$\frac{\partial x_1}{\partial t} = -a \frac{\partial x_1}{\partial z} + f_1(x_1, x_2, x_3, u) \quad (2.53)$$

$$\frac{\partial x_2}{\partial t} = -a \frac{\partial x_2}{\partial z} + f_2(x_1, x_2, x_3, u) \quad (2.54)$$

$$\frac{\partial x_3}{\partial t} = -a \frac{\partial x_3}{\partial z} + f_3(x_1, x_2, x_3, x_4, u) \quad (2.55)$$

$$\frac{\partial x_4}{\partial t} = -a \frac{\partial x_3}{\partial z} + f_4(x_3, x_4, x_5, u) \quad (2.56)$$

$$\frac{\partial x_5}{\partial t} = f_5(x_4, x_5, x_6, u) \quad (2.57)$$

$$\frac{\partial x_6}{\partial t} = f_6(x_5, x_6, u) \quad (2.58)$$

where $x_1, x_2, x_3, x_4, x_5, x_6$ represent $y_{CH_4}, y_{CO_2}, T, T_w, T_g$ and T_r respectively.

The boundary and initial conditions are:

$$x_1(z = 0, t) = y_{CH_4, in}(t),$$

$$x_2(z = 0, t) = y_{CO_2, in}(t),$$

$$x_3(z = 0, t) = T_{in}(t),$$

$$x_4(z = 0, t) = T_{w, in}(t),$$

$$x_5(t = 0) = T_{g, in},$$

$$x_6(t = 0) = T_{r, in}.$$

2.6.3 Specifying Discretisation Methods for DPS

The model equations of the system in this work are solved in gPROMS [47] and Matlab-Simulink for different purposes in this thesis. The simulations in Chapter 2 and Chapter 3 are realized in gPROMS, and the simulations in Chapter 4 are achieved in Matlab-Simulink. In fact, gPROMS can effectively deal with most complex processes that involve a combination of distributed and lumped unit operations. The equations that determine the behaviour of such unit operations are typically systems of integral, partial differential, ordinary differential and algebraic equations [48]. The solution of such systems is generally a difficult problem. Changing the value of a parameter or one of the boundary conditions may lead to completely different behaviour from that originally anticipated. Furthermore, although some numerical methods can accurately solve a given system, other numerical methods may be totally unable to do so.

The systems of partial differential, ordinary differential and algebraic equations are normally solved using numerical methods that involve discretisation techniques of the distributed parameter equations (PDEs) with respect to all spatial domains. Numerous schemes for discretising the spatial domains are provided in gPROMS [47], but only one single discretisation method can deal efficiently with all forms of equations and boundary conditions, and this preferred method is specified by the user. Three specifications (type of spatial discretisation method, order of approximation, and number of discretisation intervals/elements) are necessary to completely determine the discretisation method.

Table 2.1: Numerical methods for distributed systems in gPROMS

Numerical method	Keyword	Order of approximation
Centered Finite Difference	CFDM	low
Backward Finite Difference	BFDM	low
Forward Finite Difference	FFDM	low
Orthogonal Collocation on Finite Elements	OCFEM	low
Gaussian Quadratures		high

In this work, the first order Backward Finite Difference Method is used. Different numbers of discretisation elements have been tested and compared to solve the system of coupled differential and algebraic equations (DAEs). and the number of discretisation elements of 20 is chosen as to balance the computational load and accuracy of approximation. The model parameters and operation conditions are specified in Table 2.2 according to a primary reformer unit in an ammonia plant and literatures [18] [44] [66]. In the next two sections, both steady state and dynamic simulations are carried out to study the characteristics of the process.

Table 2.2: Model parameters for the industrial gas reformer

model parameter	value/specification	unit/note
reformer parameters		
tube length	10.3632	m
tube density	8470	kg/m^3
tube wall heat capacity	750	$J/(kgK)$
tube thermal conductivity	20.738	$W/(m^2K)$
tube inner diameter	4	inch
tube outer diameter	4.59375	inch
number of tubes	136	
catalyst bed density	1362	kg/m^3
process gas heat capacity	698.2	$J/(kg.K)$
furnace parameters		
furnace length	23.53	m
furnace width	2.2	m
furnace height	10.3632	m
wall heat capacity	1000	$J/(kg.K)$
number of burners	280	
feed parameters		
$hc(H_2/CH_4)$	0.0001	molar feed ratio
$dc(CO_2/CH_4)$	0.0072	molar feed ratio
$nc(N_2/CH_4)$	0.0041	molar feed ratio
operating conditions		
$sc(\text{steam}/CH_4)$	3	molar feed ratio
F_f	1810	$scfm$
F_p	3170	$scfm$
P_{in}	1923	kPa
T_{in}	773	K
$T_{w,in}$	1021	K
T_{amb}	300	K
burner states		(top to bottom)
line 1	[1 0]	0=off, 1=on
line 2	[1 1 1]	0=off, 1=on
line 3	[1 1]	0=off, 1=on
line 4	[1 1 0]	0=off, 1=on
line 5	[0 1]	0=off, 1=on
line 6	[1 0 0]	0=off, 1=on

2.7 Steady State Simulation and Model Validation

Using furnace parameters and unit operating conditions provided in Table 2.2, and assuming the initial conditions along each tube are the same as the boundary conditions at tube entrances, steady state simulations are performed on tubes at various locations (see blue dots in Figure 2.6).

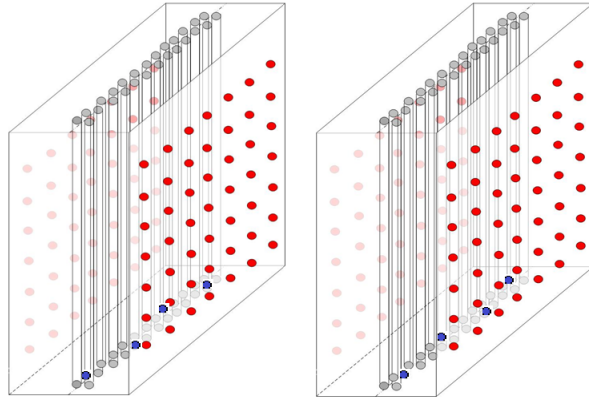


Figure 2.6: Tubes selected for model validation

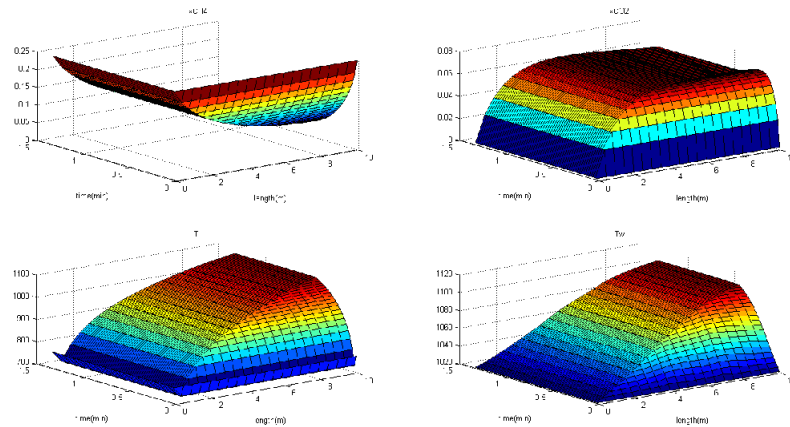


Figure 2.7: Steady states profiles along a reforming tube(top to bottom)

As the mole fractions of CH_4 and CO_2 , and temperatures of process gas and tube wall change with both time and space (along the axial direction of tubes), three dimensional plots(see Figure 2.7) are presented for steady-state simulation with given initial conditions at non-steady state.

The inlet steam/carbon ratio, feed flow rate, fuel gas flow rate, and ambient temperature are important factors in the process simulation. Any change in these factors in the reforming process occurring in the primary reformer results in changes of outlet states of mole fractions

CH_4 and CO_2 , reformed gas and tube wall temperatures. Steady state behaviour of the model is studied for different system configurations of the aforementioned five factors in this chapter.

Figure 2.8 - 2.11 provide the profiles of the four states of mole fractions and temperatures along the tube at steady state under different operation conditions of aforementioned factors. Table 2.3 - 2.6 compare the values of selected process variables to these factors.

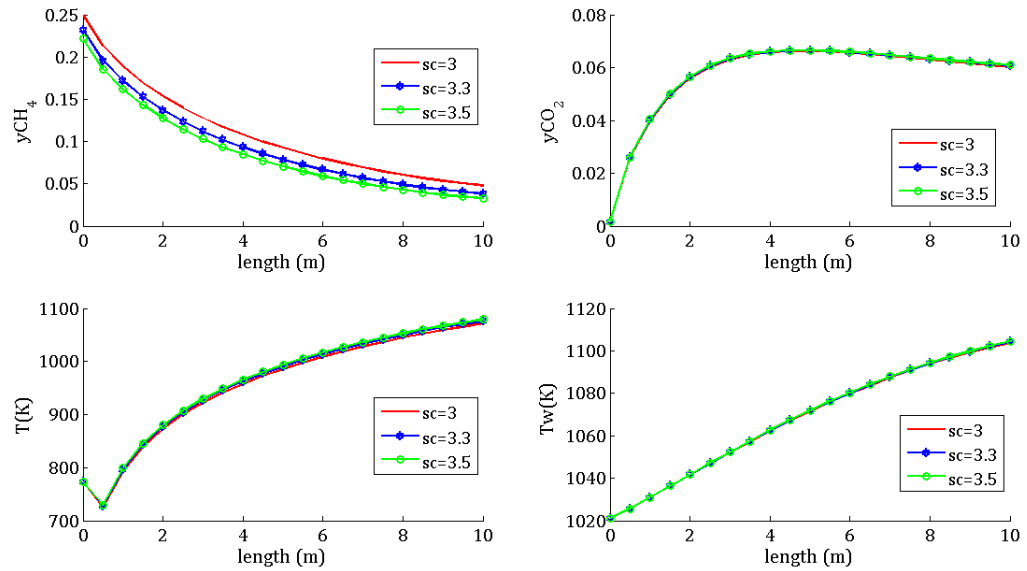


Figure 2.8: Steady states profiles of outlet states at different s/c ratios

The simulations performed are with varying steam/carbon ratio, namely: $s/c = 3$, $s/c = 3.3$, and $s/c = 3.5$. The axial profiles of reformed gas and tube wall temperatures and mole fractions of CH_4 and CO_2 are shown in Figure 2.8. Table 2.3 compares the values of process variables at different operating conditions of steam/carbon ratio. As expected the data shows that the conversion of CH_4 increases with increasing steam/carbon ratio. It is also noted that in each process gas temperature profile, there is a temperature drop at the entrance of the tube, which is caused by effect of endothermic reactions. The catalyst speeds up the endothermic reactions once the process gas flows into the tube from the entrance without receiving enough external heat to maintain its temperature. As the process gas flows further and receives more heat absorbed from the tube wall, the temperature goes up.

Table 2.3: Process variables to different operating conditions of steam/carbon (s/c) ratio

s/c ratio	y_{CH_4}	y_{CO_2}	T	T_w
3	0.0480	0.0603	1071	1103.75
3.3	0.0381	0.0607	1076	1104.20
3.5	0.0327	0.0609	1079	1104.45

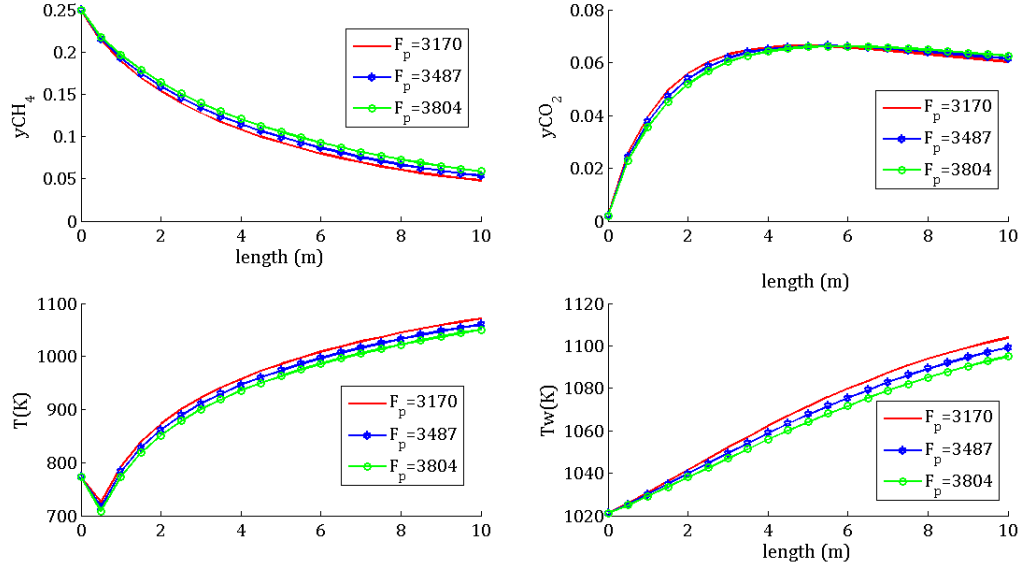


Figure 2.9: Steady states profiles of outlet states at different process gas flow rates

The simulations performed are with varying process gas flow rate (inlet), namely: $F_p = 3170$ scfm, $F_p = 3487$ scfm, and $F_p = 3804$ scfm. The axial profiles of mole fractions of CH_4 and CO_2 and reformed gas and tube wall temperatures are shown in Figure 2.9. Table 2.4 compares the values of process variables at different operating conditions of process gas flow rate. As expected the result shows that the conversion of CH_4 and reformed gas temperature decrease with increasing process gas flow rate (inlet).

Table 2.4: Process variables to different operating conditions of process gas flow rate

F_p (scfm)	y_{CH_4}	y_{CO_2}	T (K)	T_w (K)
3170	0.0480	0.0603	1071	1104
3487	0.0534	0.0615	1060	1099
3804	0.0586	0.0625	1050	1095

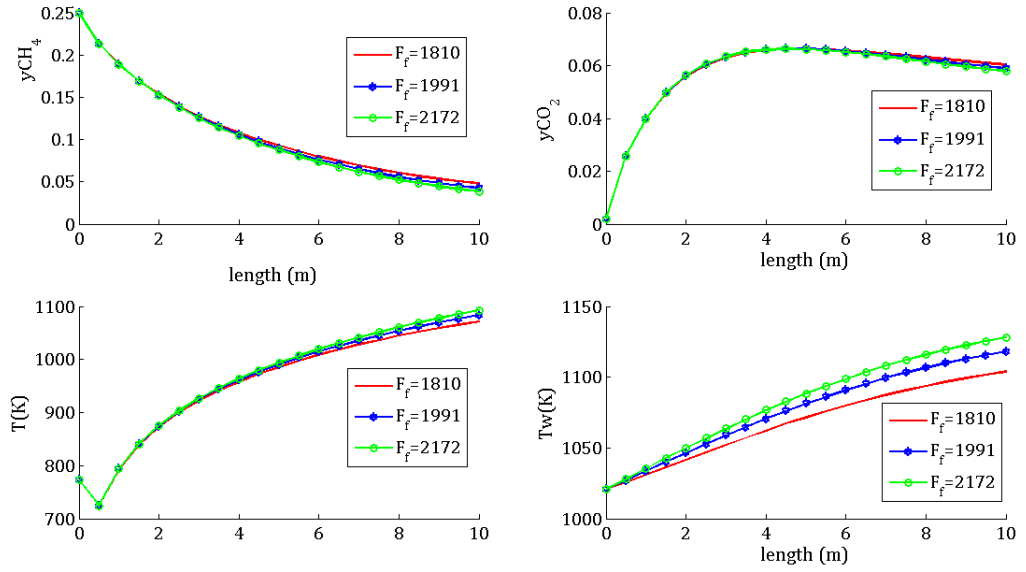


Figure 2.10: Steady states profiles of outlet states at different fuel gas flow rates

The simulations performed are with varying fuel gas flow rate (inlet), namely: $F_f = 1810$ *scfm*, $F_f = 1991$ *scfm*, and $F_f = 2172$ *scfm*. The axial profiles of mole fractions of CH_4 and CO_2 and reformed gas and tube wall temperatures are shown in Figure 2.10. Table 2.5 compares the values of process variables at different operating conditions of process gas flow rate. As expected the result shows that reformed gas and tube wall temperatures increase with increasing fuel gas flow rate (inlet).

Table 2.5: Process variables to different operating conditions of fuel gas flow rate

F_f (scfm)	y_{CH_4}	y_{CO_2}	T (K)	T_w (K)
1810	0.0480	0.0603	1071	1104
1991	0.0423	0.0589	1083	1118
2172	0.0383	0.0578	1092	1128

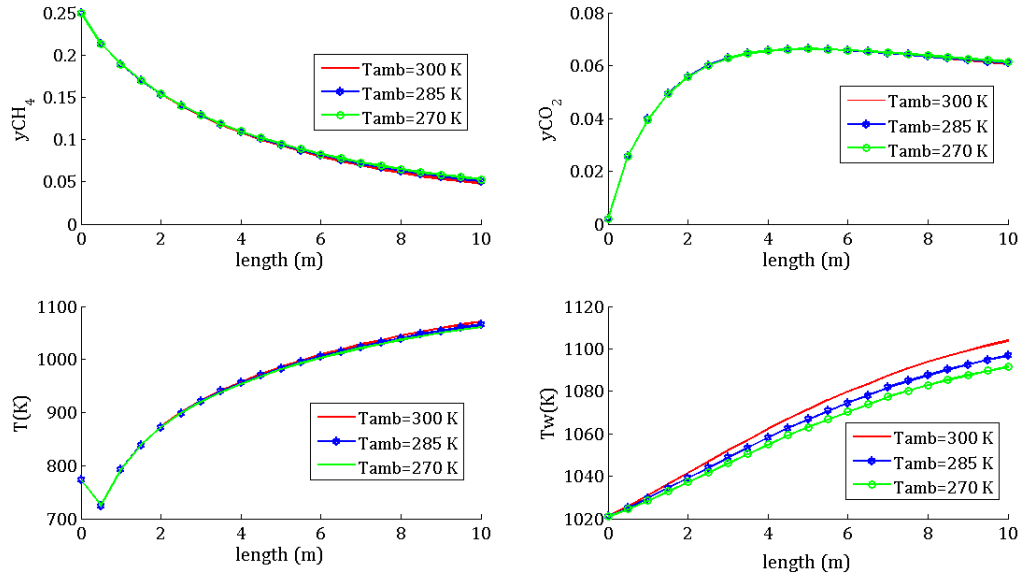


Figure 2.11: Steady states profiles of outlet states at different ambient temperatures

The simulations performed are with varying ambient temperatures, namely: $T_{amb} = 300K$, $T_{amb} = 285K$, and $T_{amb} = 270K$. The axial profiles of mole fractions of CH_4 and CO_2 and reformed gas and tube wall temperatures are shown in Figure 2.11. Table 2.6 compares the values of process variables at different operating conditions of process gas flow rate. As expected the result shows that reformed gas and tube wall temperatures decrease with decreasing ambient temperature.

Table 2.6: Process variables to different operating conditions of ambient temperature

T_{amb} (K)	y_{CH_4}	y_{CO_2}	T (K)	T_w (K)
300	0.0480	0.0603	1071	1104
285	0.0508	0.0609	1065	1097
270	0.0529	0.0614	1061	1092

Validation of the model is performed against industrial data for a side fired primary gas reformer within the ammonia process. The simulation results are presented in Table 2.7. Numerical outputs of model simulations and measured data recorded from an ammonia plant were compared and good agreement was found in absolute values. The data has been normalized for proprietary reason and the error in estimating outlet temperature of synthesis gas was found to be negligible (0.44%). Figure 2.12 is the plot for the results in Table 2.7. It shows that even though there exist gaps between model values and plant values at the eight stated locations, the simulation result entails the temperature trend

Table 2.7: Comparison between plant and simulated data (normalized)

Outlet Temperature	Plant Value	Model Value	Deviation (%)
T_1 (SW)	0.99393	0.99818	0.23
T_2 (SWC)	0.99402	0.99866	0.37
T_3 (SEC)	0.99444	0.99914	0.47
T_4 (SE)	0.99742	1	0.26
T_5 (NW)	0.99271	0.99799	0.53
T_6 (NWC)	0.99358	0.99847	0.49
T_7 (NEC)	0.99329	0.99808	0.48
T_8 (NE)	0.99732	1	0.27
T_{mean}	0.99459	0.9986	0.44

corresponding with the one in the industrial data. The model is partially validated since it is difficult to get appropriate dynamic process data from the plant. It can be seen from the comparison that the simulated data follows the overall trend of industrial data although small bias is observed.

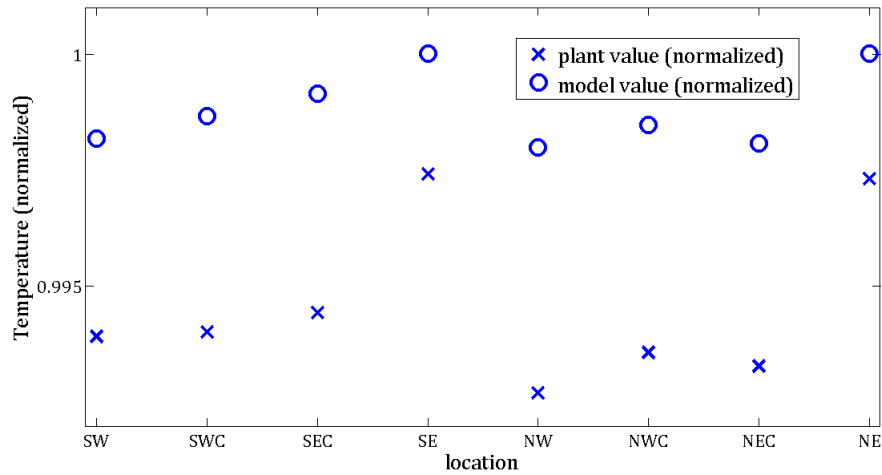


Figure 2.12: Steady state validation (normalized)

2.8 Dynamic Simulation and Discussion

Control design can be based on the mathematical models developed above, which contains PDEs coupled with ODEs; however, one can also develop a simplified model using system identification. The standard practice is to perform step tests to investigate dynamic responses of the system to input and disturbance changes. A step change of 10% of inputs' steady state value is commonly used for the gas reforming process [54], since it is large enough for the visible response. However, for the step change of the disturbance variable T_{amb} , a step change of 5 K instead of the 10% disturbance's steady state value, is chosen by the experience of plant operators. Mole fractions of CH_4 and CO_2 , and temperatures of reformed gas and tube wall along the tube are observed for the step responses. Results will be shown and discussed in this section.

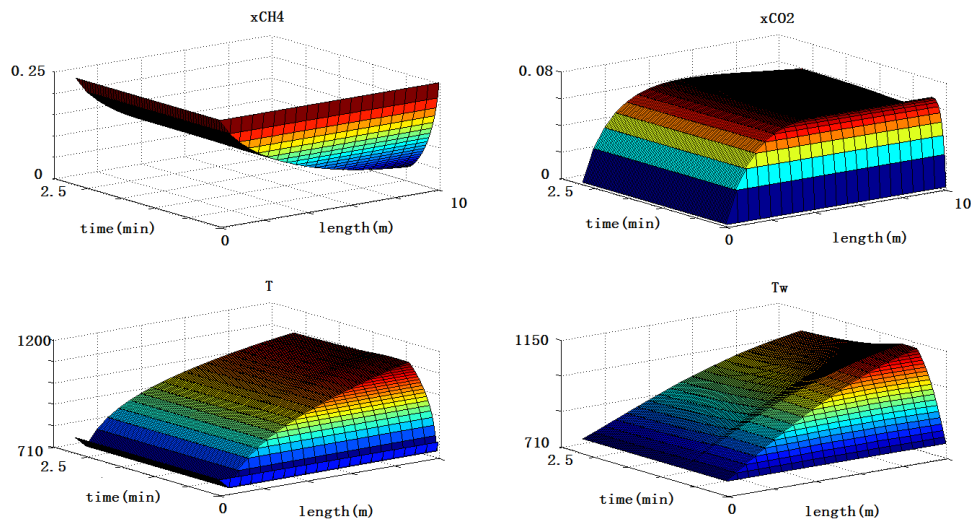


Figure 2.13: Model response to a step change in the fuel gas flow rate

A simulation is performed for a step test of fuel gas flow rate changes from 1810 *scfm* to 1629 *scfm*. The 3-dimensional profiles of selected states shows fast and smooth responses with an average settling time of 20 s (settling time varies in a small amount among the four different states). The simulation shows that the system reaches a new steady state within 20 seconds and CH_4 conversion and reformed gas temperature decrease with decreasing fuel gas flow rate.

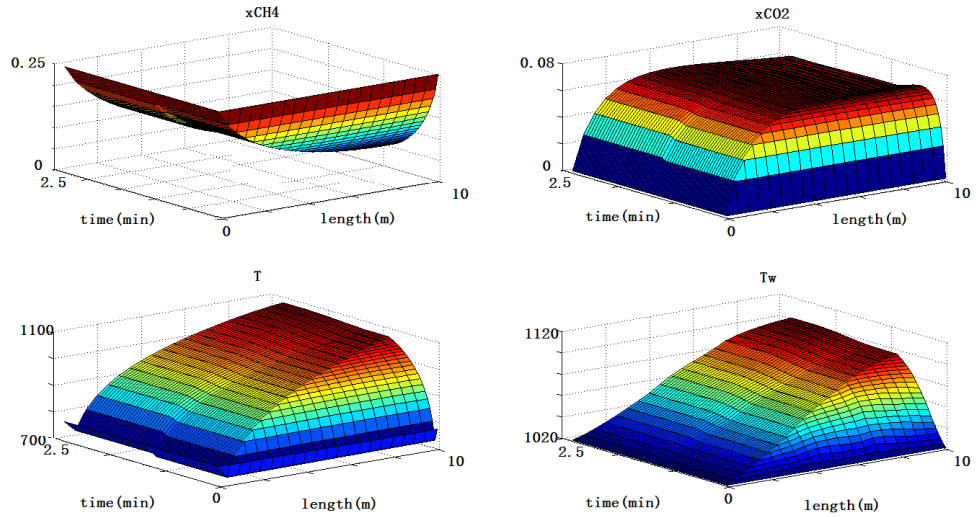


Figure 2.14: Model response to a step change in the process gas flow rate

A simulation is performed for step test of flow rate changes in process gas from 3170 *scfm* to 2853 *scfm*. The 3-dimensional profiles of selected states shows fast and smooth responses with the average settling time of 40 *s* (settling time varies in a small amount among different variables). The simulation shows that the system reaches a new steady state in a short time and with the decreasing process gas flow rate (inlet). Higher CH_4 conversion and reformed gas temperature are achieved.

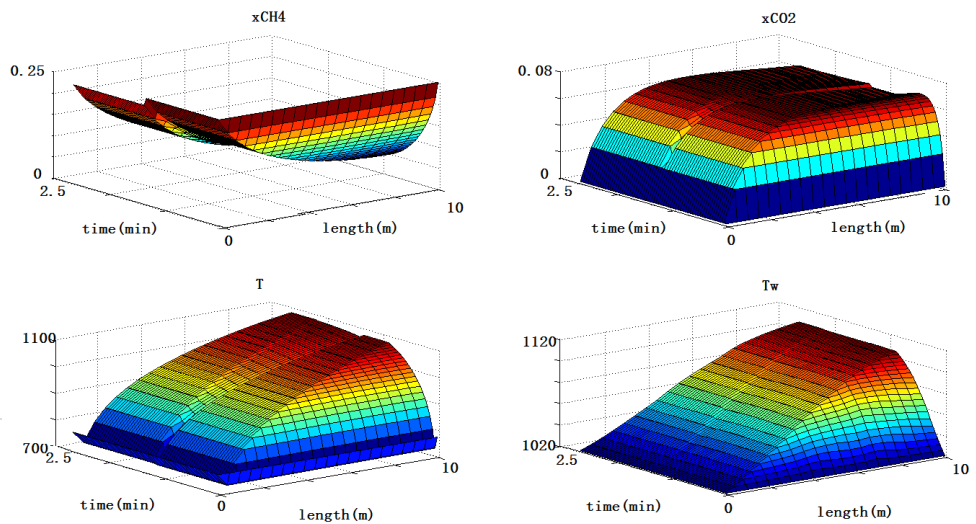


Figure 2.15: Model response to a step change in the steam/carbon ratio

A simulation is performed for step test of the steam/carbon ratio from 3 to 3.3. The

3-dimensional profiles of selected states (mole fractions of CH_4 and CO_2 , temperatures of reformed gas and tube wall) shows fast and smooth responses with the average settling time of 40 s (settling time varies in a small amount among different variables). With the increase of steam/carbon ratio, mole fractions of all components are changed, which affects all the states considered here. The simulation shows that the system reaches a new steady states in a short time and with the increasing steam/carbon ratio, higher CH_4 conversion and reformed gas temperature are achieved.

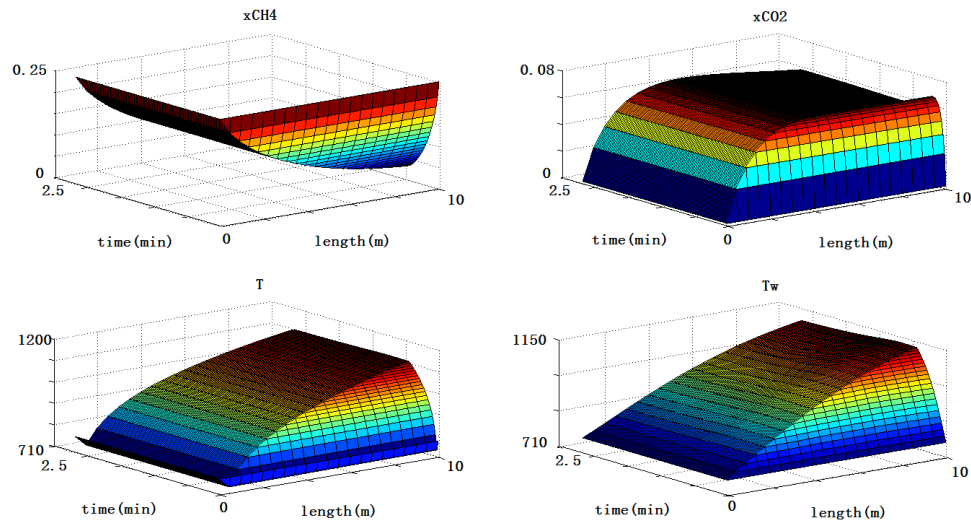


Figure 2.16: Model response to a step change in the ambient temperature

A simulation is performed for step test of the ambient temperature from 300 K to 305 K. The 3-dimensional profiles of selected states shows small but smooth responses especially the tube wall temperature change but it is difficult to identify a settling time.

Two step tests are performed to check the outlet temperature change with two burners at particular positions that are switched off one after the other. As shown in Figure 2.17, at time point 50s when burner (1,3) is switched off, the outlet temperature (T_1) of the Tube 1 which is closer to the burner (1,3) has greater temperature change than the outlet temperature (T_3) of the Tube 3. Similar results are observed when burner (3,5) is switched off at time point 100s. The time constant is approximately 3-5 seconds.

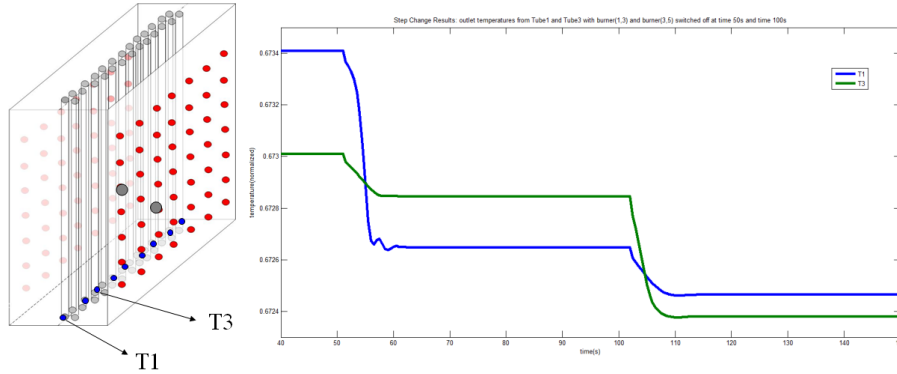


Figure 2.17: Outlet temperature profiles with side burners switched off I

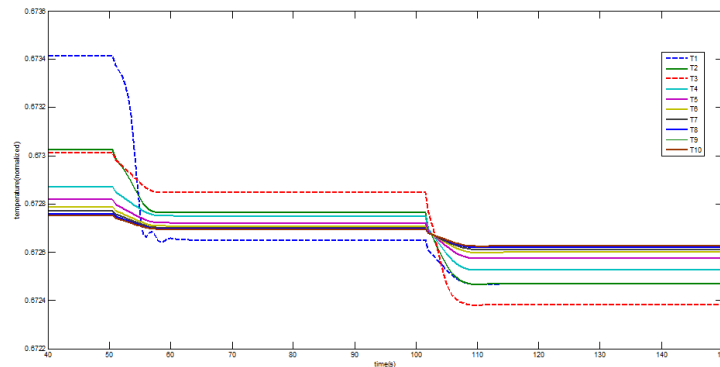


Figure 2.18: Outlet temperature profiles with side burners switched off II

From Figure 2.18, it is worth noting that when one burner is switched off the closest outlet temperature would decrease by approximately 2°F. This is not a fixed amount since burners at different elevations may have different level of influence on the reformed gas temperature. To further investigate the influence of burner switching on tube outlet temperatures, ten tubes that are evenly distributed inside the furnace are considered, where the blue dots in Figure 2.18 represent the locations of temperature measurements. Figure 2.17 illustrates the influence of burner switching on tube outlet temperatures at ten evenly distributed locations. The blue and green lines are the same profiles as the red and blue dash lines shown in Figure 2.18. From Figure 2.17, it is clear that the temperature profiles

that have great changes according to the burner switches belong to the tubes that are close to the burner that was switched off. The closer to the burner that the tube is, the greater the temperature changes. According to Figure 2.17, the farthest two tubes from the two switched burners barely have any response to the burner switches.

2.9 Conclusion

This chapter has developed dynamic mathematical models consisting of partial differential equations (PDEs) coupled with ordinary differential equations (ODEs), as well as algebraic equations. Conservation equations for mass and heat, including radiation are developed, and the model parameters are tuned against empirical data. Numerical outputs of model simulations and measured data recorded from an ammonia plant were compared and good agreement was found in overall trends. The error in estimating outlet temperature of synthesis gas was found to be small (0.44%).

The steady state modelling and analysis of a primary reformer using energy balance equations were performed considering simultaneous radiation and convection heat transfer processes and chemical reforming reactions in the presence of catalyst. The comparison of computed and measured data show the importance of parameters such as feed flow rate, steam/carbon ratio, fuel gas flow rate, and ambient temperature in methane conversion efficiency. Dynamic simulation on step changes has also provided information for input design for applying system identification methods.

The mathematical models developed from this chapter lay a foundation for system optimization and optimal control design. In the following chapters, the dynamic mathematical model is used for optimization and control design purposes by MATLAB [40] and gPROMS [47].

Chapter 3

Optimization Strategies for Burner Operation

Optimization of the reforming process involves the manipulation of some operating conditions to achieve a high process yield while maintaining low operating and equipment replacement costs. Providing plant operators and owners with the ability to achieve high yield and substantially extend tube life in gas reformers is essential in maximizing the use of capital investments in methanol, hydrogen, and ammonia plants [50]. With the price of nickel at an all time high, the cost of replacing a single reformer tube can be upwards of \$20,000 USD in today's market. Moreover, the effect of the unplanned downtime in reducing the plant on-stream factor is even greater than the installed cost of a single reformer tube. Therefore, the optimization of plant operating parameters, such as burner states, is of great importance for maximizing tube life, achieving high yield and maintaining safe operation.

As in the description of gas reformer furnace, the plant burners located on the side wall are only available for manual operation and only have two states: on or off. We use the binary integer variables (0 – 1) to represent the on/off decisions of burners (on = 1, off = 0). Such optimization problems arise in many other real world applications as well. The existence of decision variables, which take on discrete values, presents a challenge of the combinatorial nature of mixed integer programming (MIP). Another challenge in this work is that the DPS is built up with coupled quasilinear PDEs that contain non-linearities in the non-derivative terms.

The objective of this chapter is to develop optimization strategies for manipulating side-fired burners in order to provide smooth heat flux profiles that can prolong tube life and uniform reformed gas temperatures. The MINLP optimization procedure for primary gas reformer is posed and solved in gPROMS [47] and the results provide optimal operating conditions of side-fired burners. These results may provide guidance for the manual operation of side-fired burners.

3.1 Problem Formulation

Based on plant operating experience, it is known that the outlet temperature of the reformed gas is mainly affected by steam-carbon ratio (s/c ratio), fuel gas flow rate (F_f), process gas flow rate (F_p), ambient temperature (T_{amb}) and the burner states. The s/c ratio and the process gas flow rate are usually fixed in actual plant operation unless the production requirement or feedstock composition changes. In this work, these two variables are fixed but can be considered as measured disturbances to the system, should the plant operating conditions change. The fuel gas flow rate (continuous variable) and burner states (binary variables) are considered as manipulated variables in this work, which makes the optimization problem an MINLP problem. However, in this chapter, only the optimization of burner states with respect to four objective functions are considered. The fuel gas flow rate, together with burner states, are considered as manipulated variables for the dynamic optimization problem (predictive control) in Chapter 4. In addition, the uneven distribution in the ambient temperature profile caused by weather issues (i.e., a strong, long-lasting air flow of a particular direction) or partial overheating from objects nearby is considered as a measured disturbance in this chapter.

In this work, the optimization procedure is executed based on the steady-state version of the system that is derived by setting the time derivatives of all differential variables to zero. The static optimization problem is formulated as follows:

$$\begin{array}{lll} \underset{m_1, m_2}{\text{minimize}} & f(x, m_1, m_2, d) & \text{objective function} \end{array} \quad (3.1)$$

subject to

$$g(x, m_1, m_2, d) = 0, \quad \text{system's state equations} \quad (3.2)$$

$$h(x, m_1, m_2, d) \leq 0 \quad \text{process constraints} \quad (3.3)$$

$$r(x, m_1, m_2, d) = r_d \quad \text{regulatory control tasks} \quad (3.4)$$

$$d - d^* = 0 \quad \text{disturbance specifications} \quad (3.5)$$

$$m_1 \in X, \quad \text{continuous variables} \quad (3.6)$$

$$m_2 \in Y, \quad \text{discrete variables.} \quad (3.7)$$

where x is the vector of states, m_1 and m_2 are vectors of continuous and discrete manipulated variables, and d is the vector of disturbances. In this chapter, the optimization procedure is executed to find an optimal solution of burner operating conditions for a primary gas reformer based on four different objective functions, with further consideration of a constant disturbance (d) of uneven ambient temperature distribution.

With same system constraints, initial conditions and boundary conditions, four different objective functions are considered and presented as below:

$$obj1 : \min_{burner} \sqrt{(T_{ave} - T_1)^2 + \dots + (T_{ave} - T_{N_t})^2} \quad (3.8)$$

$$obj2 : \min_{burner} \frac{1}{N_t} \sum_1^{N_t} |T_{ave} - T_i| \quad (3.9)$$

$$obj3 : \min_{burner} \max\{|T_{ave} - T_i|, i = 1, 2, \dots, N_t\} \quad (3.10)$$

$$obj4 : \min_{burner} \frac{1}{N_t} \sum_1^{N_t} [(T_{wt} - T_{w,t}(i))^2 + (T_{wm} - T_{w,m}(i))^2 + (T_{wb} - T_{w,b}(i))^2] \quad (3.11)$$

s.t.

system's dynamic equations: Equation (2.37) to Equation (2.42)

initial and boundary conditions: Equation (2.43) to Equation (2.52)

process constraints:

$$1034 \text{ K} \leq T_{ave} \leq 1036 \text{ K} \quad (3.12)$$

$$F_f = 1750 \text{ scfm} \quad (3.13)$$

$$burner(i, j) = 0 \text{ or } 1 \quad (3.14)$$

where F_f is a continuous manipulated variable which represents the fuel gas flow rate*; $burner$ is a set of binary manipulated variables which represent burner states; T_{ave} is the average of outlet process gas temperatures of selected tubes; T_i is the value of outlet process gas temperature of the i^{th} tube; T_{wt} , T_{wm} , and T_{wb} are reference temperatures of tube wall at top, middle and bottom levels, and $T_{w,t}(i)$, $T_{w,m}(i)$, $T_{w,b}(i)$ are individual tube temperatures at the corresponding elevations.

3.2 Optimization Studies using gPROMS

In Chapter 1, we introduced some of the most important solution strategies for MINLP problems, such as Generalized Benders Decomposition (GBD), Branch and Bound (BB), Outer Approximation (OA), etc. These algorithms share some similarities in solving continuous NLP sub-problems, but use different approaches to find discrete optimal decision variables. In a computational study of Duran and Grossmann [15], it is proven that the OA method generally requires relatively few cycles or major iterations and predicts stronger lower bounds. For more theoretical and practical aspects of MINLP techniques, readers are referred to [24] [14] [37]. Many of the above mentioned algorithms can use existing NLP and MILP solvers as building blocks in the form of sub-solvers, which is an enormous

*The fuel gas flow rate F_f is considered as a constant in this chapter, but a variable in Chapter 4.

advantage since these solvers have all the algorithmic development that can be productive in the MINLP algorithm.

In this chapter, the model is developed using gPROMS Model Builder, which handles dynamic simulation and optimization of models with over 100,000 differential and algebraic equations [47] with various features of numerical solution methods for discretization, optimization and parameter estimation. Optimization strategies for burner operating conditions are usually carried out using steady state optimization approach with a steady state model[†]. However, in this work, much effort has been invested in building a dynamic mathematical model for the DPS, and gPROMS is a process modelling software that is well suited for the dynamic modelling, simulation and optimization of chemical processes. Dynamic optimizations are performed with special settings to achieve solutions of integer decision variables for the DPS systems. Aside from specifications of objective functions and various constraints that optimal solutions have to satisfy, some other parameters have been determined particularly: the decision variables of burner states are set as time-invariant (constant); the control horizon is set to be equal to the prediction horizon; the prediction horizon is set to be 50 sampling time ($50t_s$), which is 2.5 times than the residence time ($20t_s$) to ensure that the system reaches a state of equilibrium (the process variables appear to maintain stable values). The prediction horizon in the dynamic optimization is set to cover a large quantity of steady state values so that the minimization is geared towards the steady-state part.

3.2.1 Solution Techniques

In this work, an MINLP solver called OAERAP[‡] is used to find optimal solution for burner operating conditions. The solver has two sub solvers: SRQPD[§] is used for solving NLP problems, and GLPK[¶] is used for solving MILP problems. The solution technique used in gPROMS for optimization is called control vector parameterization (CVP), which employs a parameterization of the control variables over the control horizon. At each optimization iteration, the optimiser specifies certain values for the optimization of decision variables, an integration of the DAE system can then be performed over the time horizon to evaluate the objective function and constraints.

In addition, gPROMS also allows its user to specify various parameters that affect the numerical performance of the optimization. This is done by typically specifies various tolerances (relative and absolute DAE integration tolerance, optimization tolerance, etc.) in the SOLUTIONPARAMETERS section. The default convergence tolerance ($1e-4$) is the upper limit which is typically used. Larger values may produce inaccurate results since convergence tolerance applies to each step, and error may accumulate over a series of

[†]The Steady state model is usually obtained by setting the time derivatives in PDEs to zero.

[‡]OAERAP is short for Outer Approximation with Equality Relaxation and Augmented Penalty (see details about the outer approximation algorithm in Introduction).

[§]SRQPD is short for Successive Reduced Quadratic Programming.

[¶]GLPK is short for GNU Linear Programming Kit.

iterations when tolerance is not sufficiently tight. In this work, the convergence tolerance is set to be 1e-4 for both optimization and process simulation.

3.2.2 Error Analysis of Optimization Results

Through the optimization procedure described previously, objective functions are minimized and solutions for burner operating conditions are obtained. The DPS system achieved a state of equilibrium within the specified time horizon of $50t_s$ in the optimization procedure. For each optimization strategy, the average outlet process gas temperature T_{ave} , as a key variable in our defined objective functions, is validated against the value calculated from the states of equilibrium in the dynamic simulation results based on the burner operating solutions using *obj1* to *obj4*. The validation result is summarized in Table 3.1.

Table 3.1: Error analysis of optimization results

Average Outlet Temperature T_{ave}	<i>obj1</i>	<i>obj2</i>	<i>obj3</i>	<i>obj4</i>
Optimization Results	1034.8	1034.9	1034.3	1034.6
Simulation Results	1034.3	1034.4	1034.0	1034.1
Deviation	0.5	0.5	0.3	0.5

As the convergence tolerance for optimization is set to be 1e-4, the numerical results have four significant figures, which implies the estimated error for the average outlet temperature is 1 K. From Table 3.1, for each optimization strategy, it is seen that the deviation between optimization and simulation results is less than 1 K, which makes the numerical error negligible.

3.2.3 Comparison of Different Optimization Strategies

In order to determine the most suitable burner operating conditions, we used the MINLP solver in gPROMS to carry out the optimization procedure of OA algorithm based on four different objective functions (*obj1* to *obj4*). Dynamic simulations are performed based on these solutions, as well as an all-burner-on strategy and a typical plant operating strategy (derived from real plant burner states data**), until the dynamic systems reach a state of equilibrium. In Figure 3.1, the process gas outlet temperatures at the state of equilibrium are plotted, based on different burner operating strategies.

Process gas outlet temperatures at different locations (West (W), West-Centre (WC), East-Centre (EC), East (E)) are shown in Figure 3.1 in terms of different burner operating strategies. It is seen that, the average process gas outlet temperature obtained from the all-burner-on method exceed the upper temperature limit. This problem can be resolved by decreasing the fuel gas flow rate without changing the burner states. But given that fuel

**Current burner control strategy is developed from operators' years of experience.

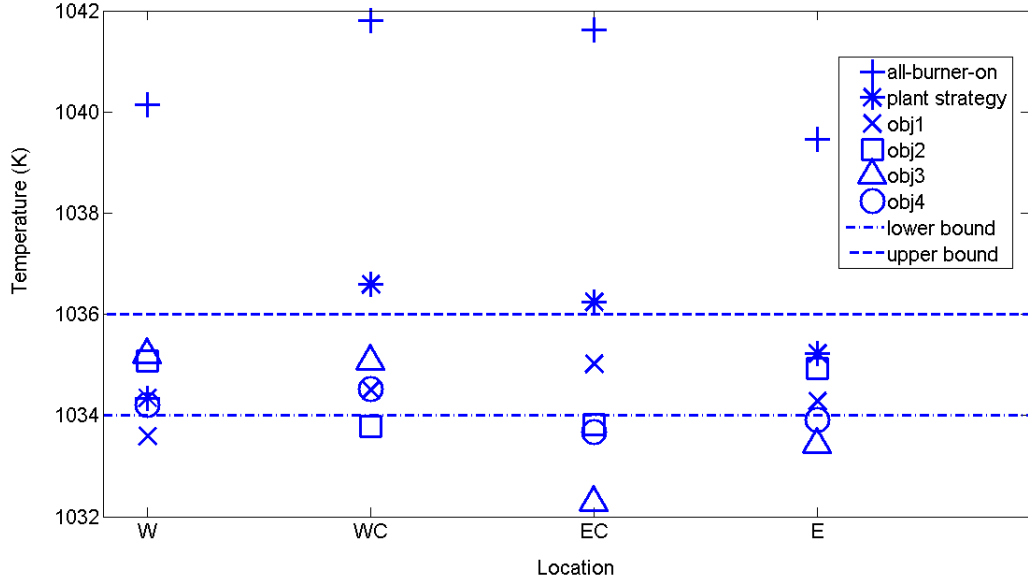


Figure 3.1: Process gas outlet temperatures from different burner operating strategies

gas flow rate cannot be manipulated in this chapter, some burners have to be switched off in order to maintain the average temperature within the constraints. The rest of burner operating strategies provide the results that can satisfy the average temperature constraints. However, from Figure 3.1, it is hard to measure how close the values of T_{out} at different locations are to each other, neither is it possible to tell which strategy is the best. In the following several paragraphs, a criteria called Root Mean Square Difference (RMSD) is introduced to analyse: the degree of smoothness in heat flux profile, uniformity of process gas outlet temperatures and uniformity of tube wall outlet (bottom) temperatures. Results from different strategies of burner operating conditions are compared and discussed.

The Root Mean Square Difference (RMSD) explains the uniformity of a set of data takes the following form:

$$RMSD = \sqrt{\frac{1}{N} \sum_{i=1}^N (x_i - \bar{x})^2}. \quad (3.15)$$

RMSD represents a kind of average deviation of a data set, which has the same unit as its data. In the data set, the closer the values are to each other, the smaller RMSD it shows. However, sometimes the RMSD seems large due to the large values of the data itself. To resolve this problem, the coefficient of variation (CV) of the RMSD, defined as the RMSD normalized to the average of the observed values, is used in this work, taking the following form:

$$CV = \frac{RMSD}{\bar{x}}. \quad (3.16)$$

The reason for listing both RMSD and CV is that for some variables, it is easier to compare using RMSD and for others it is easier using CV.

Table 3.2: Comparison between optimization results

		all- burner-on	plant strategy	<i>obj1</i>	<i>obj2</i>	<i>obj3</i>	<i>obj4</i>
RMSD	H_f	120.1	119.2	133.4	138.0	185.2	104.0
	T_{out}	1.140	1.018	0.593	0.696	1.400	0.370
	$T_{w,out}$	1.812	2.627	1.641	2.316	2.690	1.219
CV ($\times 10^{-3}$)	H_f	2.618	2.672	3.017	3.115	4.199	2.354
	T_{out}	1.095	0.983	0.573	0.672	1.354	0.358
	$T_{w,out}$	1.109	1.034	0.580	0.698	1.402	0.350

From Table 3.2 and Figure 3.1, we can draw the following conclusions:

The RMSD value of heat flux for all the burner operating strategies are not so significant compared to the large values of H_f itself (more than $45,000 \text{ kJ/h/m}^2$) with only 0.24% to 0.42% of CV, which means that there is no large variation in the heat flux profiles. Therefore, the heat flux profiles for all strategies are considered smooth. However, the better solutions are expected to produce heat flux profile with relative lower RMSD and higher uniformity.

The all-burner-on method and plant strategy have the similar RMSD in the heat flux (with only 0.9 kJ/h/m^2 difference in RMSD and 0.1% in CV), which means that both methods have the similar degree of smoothness in the heat flux profile. However, the outlet temperature average using the all-burner-on method exceed the upper temperature limit by more than 4 K , which makes the all-burner-on method not an ideal solution. The plant strategy provides relatively smooth heat flux profile, but the variance in the tube wall outlet temperatures is still relatively high.

Although *obj1* strategy achieved the second lowest RMSDs in T_{out} and in $T_{w,out}$, the heat flux profile is not the second smoothest among the selected strategies (all-burner-on strategy gives the second lowest RMSD in H_f). This is caused by the formation of its objective function in which only the uniformity of process gas outlet temperature is taken into account. Similar situations occurred to *obj2* and *obj3* strategies: due to the only consideration of outlet temperature uniformity in the objective functions, RMSDs in H_f are higher compared to all-burner-on method and plant strategy. In fact, the RMSDs in *obj2* are slightly higher than the ones in *obj1* due to the similar formulation in the objective functions. The *obj3* strategy provides us with the worst result among the selected strategies. This is due to a lack of comprehensive consideration of variable selections in its objective function (only the difference between maximum and average process gas outlet temperatures is considered to be minimized).

The proposed optimization strategy obtained by objective function *obj4*, which considers the uniformity of tube wall temperatures at three different elevations, yields the most uniform heat flux profile and outlet temperature results among all the selected burner operating strategies.

3.3 Disturbance Effects

In this chapter, the study of optimization strategy is directed towards the guidance of the manual operation of side-fired burners. For primary gas reformers, possible disturbances may include uneven distribution of process gas flow rates, fuel gas flow rates, steam/carbon ratios and/or ambient temperatures, most of which are not measurable in the plant, with the exception of ambient temperatures. In this chapter, unevenly distributed ambient temperatures is considered as a measured disturbance to the system. Weather issues (wind, rain or snow with strong, long-lasting airflow to a specific direction) or partial overheating from objects nearby can be the possible causes for this uneven distribution. In the following example, a constant disturbance of unevenly distributed ambient temperatures with a horizontal temperature gradient of 2 K (see Figure 3.2) in the west side of the furnace has been modelled. The disturbance effects are studied and the optimization strategy is carried out in regards to the constant disturbance.

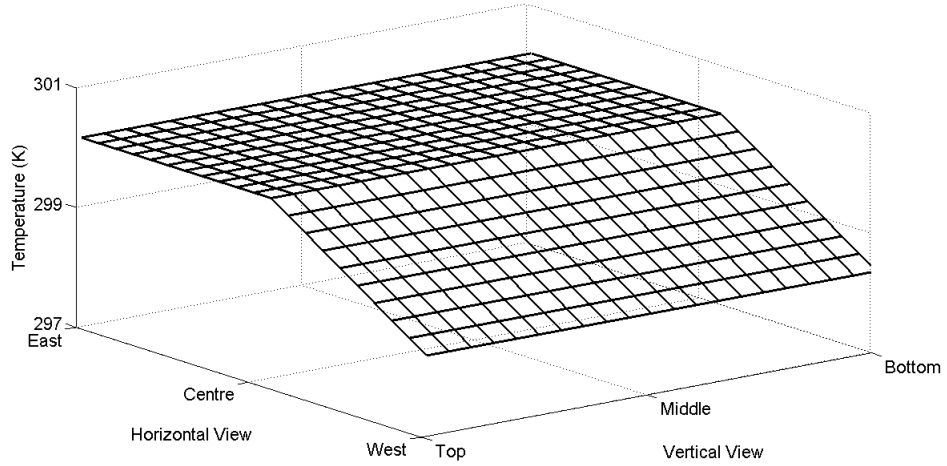


Figure 3.2: Ambient temperature profile along the refractory wall

From Figure 3.3, we can see that the process gas outlet temperatures have been affected by the constant disturbance of the uneven distribution of ambient temperature, as the temperatures at locations WC (west centre) and W (west) are 0.3 K and 1.1 K deviated from the average value of outlet temperatures. The simulation is based on the *obj4* burner operating strategy, and the RMSD of T_{out} in this scenario of system with a constant disturbance is 0.763 (higher than the RMSD of 0.370 in the case without any disturbance). Optimization procedure is carried out for this case using the objective function of *obj4*, the solution for burner operating strategy is adjusted. Dynamic simulation using the adjusted solution of burner operating strategy is performed till the system reaches a state of equilibrium. From the simulation result, it can be seen that the outlet temperatures from the west side of furnace are adjusted closer to the average value. The RMSD of T_{out} with the

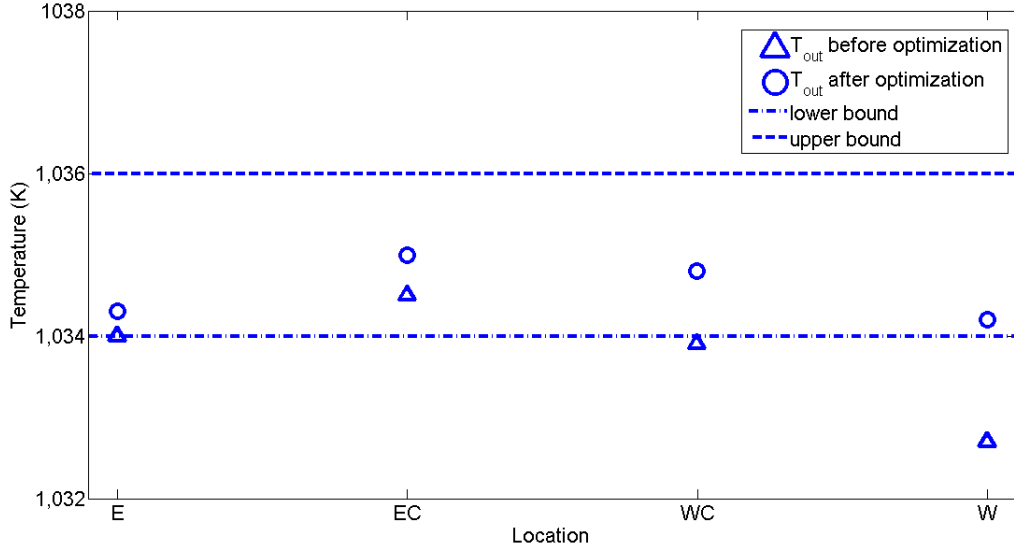


Figure 3.3: Process gas outlet temperature before and after optimization with a constant disturbance

adjusted optimization strategy in regards to the constant disturbance becomes 0.386.

3.4 Conclusion

An MINLP based optimization approach has been developed for the uniformity of outlet temperatures in a steam reforming process using gPROMS Model Builder [47]. The process model used in this chapter for optimization studies is the same as the dynamic model developed from Chapter 2, which consists of four partial differential equations and two ordinary differential equations accompanied by a set of algebraic equations. Dynamic optimizations are performed based on four different objective functions with focuses on temperature uniformity. Special settings are specified to ensure that the system reaches a state of equilibrium within a time horizon of optimization, in which the decision variables of burner states are set to be time-invariant (constant), such that the dynamic optimization solutions can be applied as an industrial guidance of burner operating strategies. A criteria called Root Mean Square Difference (RMSD) has been introduced to analyse three aspects of the system: the degree of smoothness in heat flux profile, uniformity of process gas outlet temperatures and uniformity of tube wall outlet (bottom) temperatures. Results from different strategies of burner operating conditions have been compared and discussed. A constant disturbance of unevenly distributed ambient temperatures with a horizontal temperature gradient of 2 K (see Figure 3.2) in the west side of the furnace has been modelled. The disturbance effects are studied and the optimization strategy is carried out in regards to the constant disturbance.

Chapter 4

Model Predictive Control (MPC) of Outlet Temperatures

Dynamic behaviour of the primary gas reformer is dominated by convective and radiative transfer, reaction kinetics and the bulk motion of the gas. As a result, the diffusion effects are negligible in comparison to convection effects, and the primary gas reformer is modelled by a set of coupled hyperbolic PDEs, ODEs and AEs. Compared to parabolic PDEs, the spatial differential operators of hyperbolic PDEs contain eigenmodes of the same or nearly the same amount of energy [25]. Therefore, the analysis of the infinite-dimensional nature of hyperbolic systems is required. Research conducted in the development of control approaches exploring the infinite-dimensional nature of hyperbolic systems has become increasingly active [56] [55] [29] [65] [10] [9] [28]. However, the use of MPC methods to control such systems has not been fully explored [25], especially the development of MPC schemes that exhibit higher levels of performance with better handling of constraints.

MPC is an optimal control technique that considers a multi-variable process, by solving a finite horizon optimal control problem at each sampling instant. Unfortunately, research on MPC in controlling mixed lumped and distributed parameter systems is relatively sparse. Most researchers solve the problem by using dynamic programming [59] [60] or finite difference approximation [53] approaches, in which the control of hyperbolic DPS is achieved by approximating DPS with LPS. Dubljevic et al. [53] used a finite difference method to convert the hyperbolic equations to a set of ODEs and MPC is designed for the resulting model. Karafyllis and Daoutidis [32] employed a finite difference approximation for the spatial derivatives of hyperbolic PDEs, and developed a non-linear controller for hot spot temperature control in plug-flow reactors (PFRs).

In this chapter, a temperature control problem for a side-fired primary gas reformer is considered. A non-linear Characteristic-Based Model Predictive Control (CBMPC) approach is applied to control the temperature of the reactor at the desired set-point. Numerical simulations are conducted using a detailed dynamic model of the primary gas reformer and results show that CBMPC possesses both computational efficiency and accurate performance. A conventional MPC approach is applied to an approximate lumped linear model

for the DPS developed using system identification. Simulation results indicate that the conventional MPC exhibits good performance in regulatory and set-point tracking.

4.1 Characteristic-Based Model Predictive Control

In Chapter 1, we introduced the background knowledge of Model Predictive Control and Method of Characteristics separately. In this section, an Characteristic-Based Model Predictive Control (CBMPC) scheme for output regulation is designed for the dynamic system of a primary gas reformer, which is a first-order hyperbolic multivariate system with one single characteristic. For the system prediction in CBMPC design, the Method of Characteristics technique is used for handling mathematical complexity arising from PDEs. The prediction approach is then reformulated into the NMPC algorithm, where optimal control action is calculated and implemented into the system.

The DPS studied in this work is a multivariate system where multiple dependent variables are required for the dynamic modelling. The following equations are shown as an example for the four coupled hyperbolic PDEs in the dynamic model of a primary gas reformer:

$$\frac{\partial x_1}{\partial t} + a_1 \frac{\partial x_1}{\partial z} = f_1(x_1, x_2, x_3, x_4, u) \quad (4.1)$$

$$\frac{\partial x_2}{\partial t} + a_2 \frac{\partial x_2}{\partial z} = f_2(x_1, x_2, x_3, x_4, u) \quad (4.2)$$

$$\frac{\partial x_3}{\partial t} + a_3 \frac{\partial x_3}{\partial z} = f_3(x_1, x_2, x_3, x_4, u) \quad (4.3)$$

$$\frac{\partial x_4}{\partial t} + a_4 \frac{\partial x_4}{\partial z} = f_4(x_1, x_2, x_3, x_4, u) \quad (4.4)$$

$$y = x_3(z_{max}) \quad (4.5)$$

where $x = [y_{CH_4}, y_{CO_2}, T, T_w]$ is the state variable, $y = T_{out}$ is the process output. As in the dynamic model of a primary gas reformer, we have $a = a_1 = a_2 = a_3 = a_4$, the DPS has only one single characteristic curve:

$$\text{Characteristic } C : \frac{dz}{dt} = a \quad (4.6)$$

and the state variables x_1, x_2, x_3 and x_4 are described by the following equations along the characteristic curve:

$$\frac{dx_1}{dt} = f_1(x_1, x_2, x_3, x_4, u) \quad \text{along } C \quad (4.7)$$

$$\frac{dx_2}{dt} = f_2(x_1, x_2, x_3, x_4, u) \quad \text{along } C \quad (4.8)$$

$$\frac{dx_3}{dt} = f_3(x_1, x_2, x_3, x_4, u) \quad \text{along } C \quad (4.9)$$

$$\frac{dx_4}{dt} = f_4(x_1, x_2, x_3, x_4, u) \quad \text{along } C. \quad (4.10)$$

The characteristic ODEs (Equations (4.7) to (4.10)) are non-linear. The future state variables obtained from numerical integration of characteristic ODEs is decoupled for each spatial point and prediction time instant. Assuming that the value of the current i th state variable at the spatial point z_0 is $x_{i,0}(z_0)$, the output at a future time instant can be obtained by simultaneously integrating the characteristic ODEs of the PDE model with initial conditions $t(0) = t_0$, $z(0) = z_0$ and $x_i(0) = x_{i,0}(z_0)$:

$$t = t_0 + \Delta t \quad (4.11)$$

$$z = z_0 + a\Delta t \quad (4.12)$$

$$x_1 = \int_{t_0}^t f_1(z_0, x_{1,0}, u) d\tau = \phi(z_0, x_{1,0}, u, \Delta t) \quad (4.13)$$

$$x_2 = \int_{t_0}^t f_2(z_0, x_{2,0}, u) d\tau = \phi(z_0, x_{2,0}, u, \Delta t) \quad (4.14)$$

$$x_3 = \int_{t_0}^t f_3(z_0, x_{3,0}, u) d\tau = \phi(z_0, x_{3,0}, u, \Delta t) \quad (4.15)$$

$$x_4 = \int_{t_0}^t f_4(z_0, x_{4,0}, u) d\tau = \phi(z_0, x_{4,0}, u, \Delta t). \quad (4.16)$$

The control objective in this work is to meet a set-point for the process gas outlet temperature by manipulating the fuel gas flow rate and burner states. The control action is calculated to minimize the objective function:

$$J = \sum_{i=1}^{T_p} (\hat{y}(t_i) - r(t_i))^T Q(i) (\hat{y}(t_i) - r(t_i)) + \sum_{j=1}^{T_c} (u(t_j) - u(t_{j-1}))^T R(j) (u(t_j) - u(t_{j-1})) \quad (4.17)$$

s.t.

system's dynamic equations: Equation (2.37) to Equation (2.42)

initial and boundary conditions: Equation (2.43) to Equation (2.52)

process constraints:

$$1700 \text{ scfm} \leq F_f \leq 1900 \text{ scfm} \quad (4.18)$$

$$0 \leq bn \leq 1 \quad (4.19)$$

where r is the reference signal/set-point, \hat{y} is the model prediction (process gas outlet temperature T_{out}), u is the manipulated variable (fuel gas flow rate F_f and burner states bn), Q and R are diagonal weighting matrices on system states and inputs.

In this chapter, due to the symmetry property of the furnace, one quarter of the furnace is considered for optimal control design and fifteen burner states are selected as manipulated variables. The prediction horizon is chosen to be equal to $T_p = 22t_s$, which is both dynamically and computationally adequate. The control horizon is chosen as $T_c = 4t_s$. The tuning parameters Q and R are 1000 and 0.0001 respectively. The sampling time is taken as $t_s = \frac{L}{mu_t}$, in which $m = 20$ (20 evenly distributed spacial points in the z-space are chosen

for output prediction sampling purposes). The values of all initial states are obtained from the simulation result in Chapter 2.

The prediction horizon T_p needs to be chosen long enough to capture the non-linear dynamic characteristic of the process. As we have discussed in the dynamic modelling section of the thesis, outlet temperature is significantly sensitive to radiation heat flux, and burner switches are the main factors for the variation of heat flux profile. Therefore, the selected prediction horizon should capture this rapid variation in the dynamics of heat flux profile, which, in this case, should be slightly longer than residence time (the time it takes for the synthesis gas to flow from the inlet to the outlet of the tube reactor) which is $20t_s$. Prediction horizon less than this value leads to an infeasible optimization problem: state and control constraints are either violated or system has suffered from poor performance [55].

The control algorithm is initialized with a proper selection of the initial guesses for the control signals. In this case, we assign the initial guesses to 16 manipulated variables: fuel gas flow rate F_f and 15 burner states bn . Then the optimization algorithm minimizes the pre-defined cost function by adjusting the manipulated variables in the control space. As described in the method of characteristics, optimization of the distributed parameter system is operated together with an ordinary differential equation solver at each spacial point. At $t = 0$, initial guesses are passed to ODE solver (ode15s) and the process is simulated at each of the spacial points along the prediction horizon for $T_p = 22t_s$. The simulation results pass to the SQP algorithm and this algorithm adjusts the input variables until the minimum cost is achieved within the particular time instant. This routine is repeated many times at each sampling instant until a local minima or the maximum number of iterations is achieved. When the optimal input sequence is found, the first part of the control signal is applied to the process and this input value is used to initialize the optimization algorithm at the next sampling instant. This routine is repeated until the end of the simulation.

In the simulations, number of maximum iterations is chosen to be 5 in the SQP algorithm in order to reduce computational cost of the NMPC problem and ensure the performance of the process control. The effects of how the choice of the number of iteration affects the resulting optimal control problem has been studied in literatures [33] in terms of meeting different operational performances, computation time and cost function minimization. The Simulink model is developed, with full states known at each time instant serving as initial states in the predictive controller.

For reference purpose of this chapter, the values of sampling time and residence time listed below:

- Sampling time: $t_s = 0.0217 \text{ min}$.
- Residence time: $t_r = 20t_s = 0.434 \text{ min}$.

4.1.1 Set-point tracking

The output set-point tracking response of the primary gas reformer to a set-point change from 1105 K to 1100 K at time 0.6 min is evaluated.

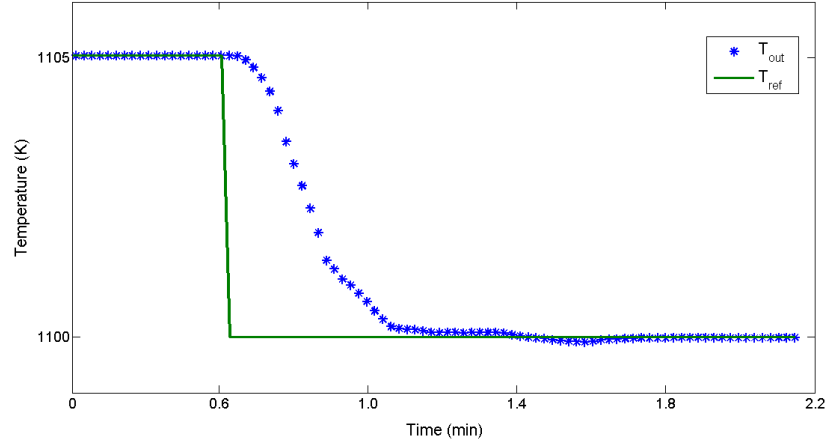


Figure 4.1: Set-point tracking response of CBMPC

From Figure 4.1, it can be seen that the CBMPC controller forces the output to track the set-point change for about one residence time (0.6 min to 1 min), adjusted for plant-model mismatch beyond the residence time for about $5t_s$ (1 min to 1.1 min), and compensated the effect of the temperature decrease on conversion for about one residence time (1.1 min to 1.5 min).

Figure 4.2a and Figure 4.2b depict the profiles of obtained optimal control signals: fuel gas flow rate F_f and 15 burner states bn .

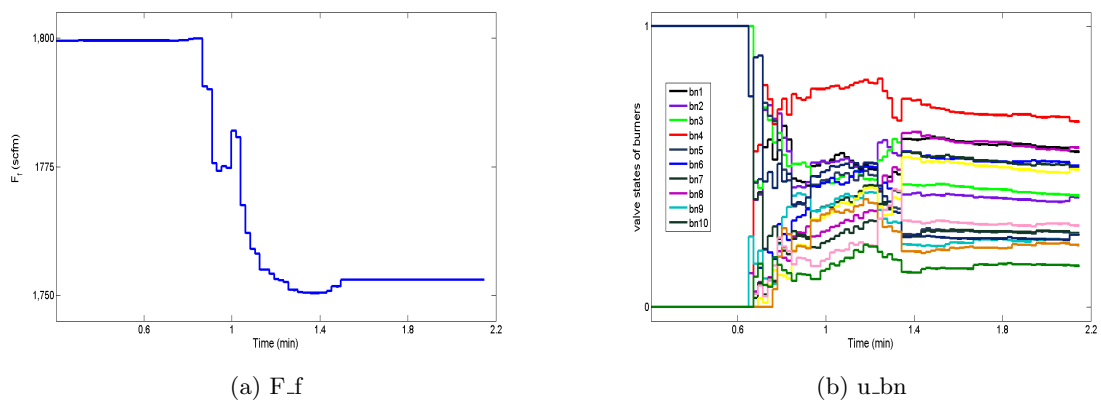


Figure 4.2: Control signals of fuel gas flow rate and burner states

It is noted that, in the CBMPC design, the optimal control signals for burner states are assumed to be continuous variables that satisfy $bn \in [0 \ 1]$, which can be seen as the valve opening of the burners. It is an ideal value and may not be implemented in the on-line systems of the plants if the burners are manually operated as "open" and "close". Nevertheless, this simulation result provides what can be expected from an optimal control if the burner opening can be changed continuously.

In general, the result of set-point tracking response shows that the proposed CBMPC controller yields smooth and fast set-point tracking response with reasonable control action.

4.1.2 Regulatory behaviour

Figure 4.3 depicts the outlet temperature response to a disturbance change of the ambient temperature T_{amb} from $300K$ to $295K$ at 0.6 min .

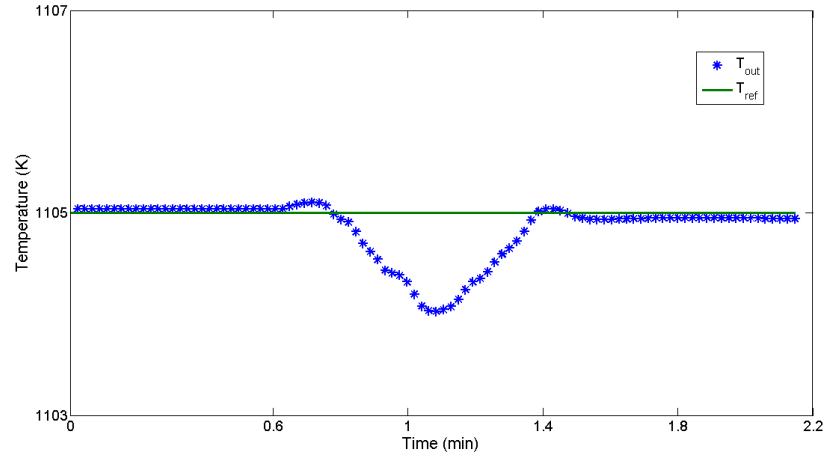


Figure 4.3: Disturbance rejection of CBMPC

From Figure 4.3, it can be seen that: from time 0.6 min to 0.8 min , the outlet temperature exhibits a small oscillatory behaviour due to an externally generated disturbance effect in ambient temperature; the output then deviates from the set-point for about one residence time (0.8 min to 1 min) due to the decrease of ambient temperature; and from 1 min to 1.1 min , the output continues to be affected by the prevailing climatic conditions; starting from 1.1 min to 1.6 min , the controller takes corrective actions to regulate the output to the set-point.

In addition, it is noted that there exists some small offset (deviation from set-point) in the control behaviour of disturbance rejection. This can be resolved by changing the term of input u into input change Δu in the objective function (4.17).

Figure 4.4a Figure 4.4b depict the profiles of obtained optimal control signals of fuel gas flow rate and burner states. The result of burner states is ideal and may not be implemented directly for on-line systems.

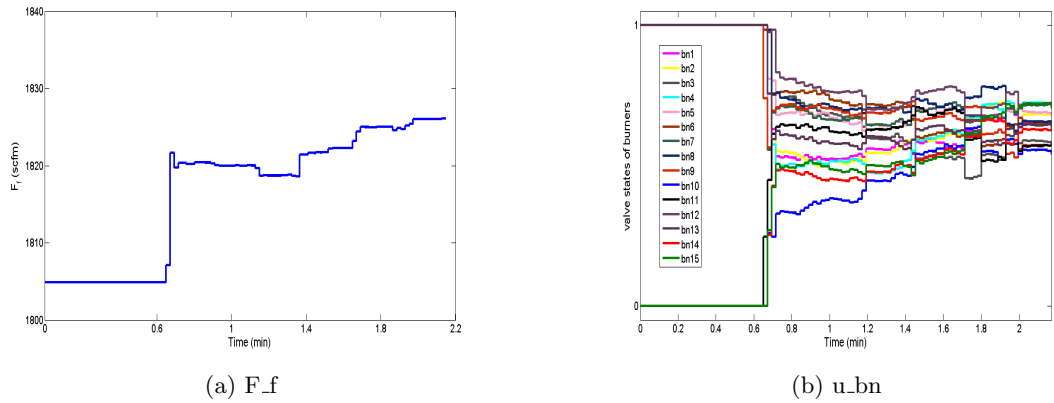


Figure 4.4: Control signals of fuel gas flow rate and burner states

Generally, the result of regulatory behaviour shows that the proposed CBMPC controller yields a good performance in disturbance rejection.

4.2 A Conventional MPC

A conventional MPC based on approximate lumped prediction models is developed in this section using system identification technique. In order to determine the discrete time transfer functions, input sequences are designed from step response tests implemented on the first-principle dynamic process model developed in Chapter 2, and system identification techniques are applied using the simulated experimental data to obtain a dynamic model that gives best approximation for the real dynamic system. Model predictive controller is designed based on the prediction model obtained from early-lumping approximation, and is then used to control the process gas outlet temperature simulated from the first-principle dynamic process model developed in Chapter 2. Different from CBMPC, in the design of this conventional MPC, 1) the output noise has been introduced to the system; 2) five rather than fifteen burner states are selected as inputs to reduce the control complexity and computer load; 3) state observer is designed for the state estimation of the system.

The system to be identified is a Multi-Input Single-Output (MISO) system, with six inputs including fuel gas flow rate and five burner states and one output being process gas outlet temperature. Six corresponding step tests are firstly implemented to obtain six continuous-time, first order plus dead time (FOPDT) model. Random binary sequences are designed from FOPDT to estimate an approximate local dynamic model. Experiments are run to obtain inputs and outputs for identification. Several system identification methods (spectral analysis, ARX, ARMAX, BJ, OE and PEM, and State Space Model) are attempted using the experimental data, and through the comparison of the residual tests, the model that provides the best description of system dynamics is chosen for controller design. Figure 4.5 gives a detailed description for the procedure of system identification.

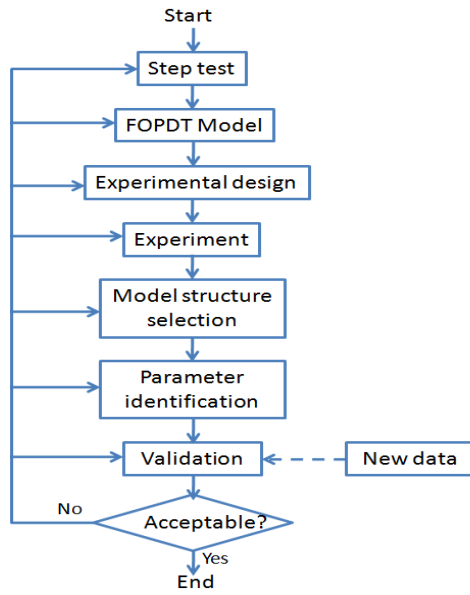


Figure 4.5: Flow chart of system identification

Box-Jenkins (BJ) model is selected as the final model structure for identification, which has the following form,

$$y_t = \frac{B(z^{-1})}{F(z^{-1})} u_{t-k} + \frac{C(z^{-1})}{D(z^{-1})} e_t. \quad (4.20)$$

To ensure the quality of the lumped model, the following procedure is followed: 1) time delay is determined by checking impulse response; 2) the order of each parametric polynomial in each model all starts from the first order; then the auto-correlation and cross-correlation tests are applied; if it passes all tests the model order is determined; 3) at last the infinite-step prediction performance is examined to ensure the model is in good fit; 4) model prediction result is compared with validation data to check the predictability of the model.

In system identification, it is traditional to split the data into two parts: two thirds is called training data, and the rest is for validation purposes [30] [38] [57]. Figures in 4.6 to 4.9 present the results of impulse response, residual tests, and infinite-step prediction performance.

1) Impulse response

Figures in 4.6 show the results of impulse response, by checking which the time delay for is determined. One can see from Figure 4.6 that for each individual test of impulse response from one input to one output, the time delay is two sampling time ($2t_s$), which is 1/10 of the residence time ($20t_s$).

2) Residual tests

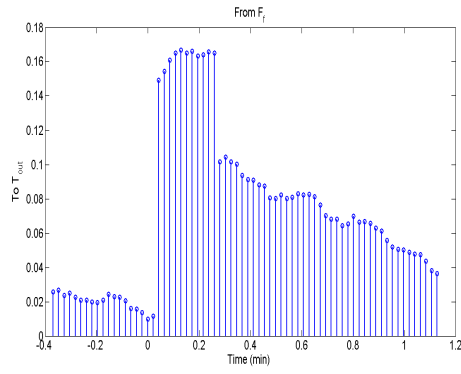
Figures in 4.7 show the results of residual tests, from which the model orders are determined and validated by checking their auto-correlation and cross-correlation tests. The procedure of the determination of model orders from residual tests is summarized as follows: 1) order of each parametric polynomial in each model all starts from the first order; 2) then the auto-correlation and cross-correlation tests are applied; 3) if it passes all tests the model order is determined; otherwise the order is increased by one and the steps 1) and 2) are repeated. However, as shown in most of the figures in 4.7, there is some violation (small percentage) in the auto-correlation and cross-correlation tests, which is negligible compared to the significantly increased model orders otherwise. The result of model orders can be found in Equation (4.21).

3) Infinite-step prediction performance

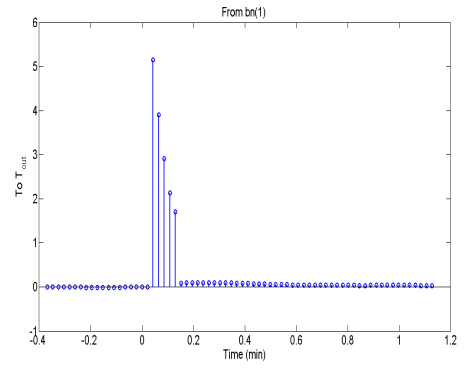
Figures in 4.8 show the results of infinite-step prediction performance, in which one can see that the model is in good fit with high percentage of data-matching between prediction data and training data. However, the predictability cannot be proven through this test but through infinite-step prediction validation.

4) Infinite-step prediction validation

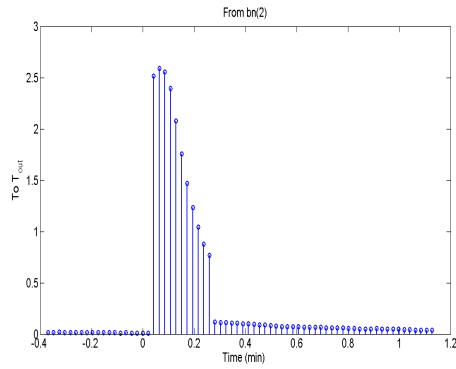
Figures in 4.9 show the results of infinite-step prediction validation, in which model prediction result is compared with validation data to check the predictability of the model. From the validation results, we can conclude that the model has good predictability proven by good fitting performances in the infinite-step prediction validation results.



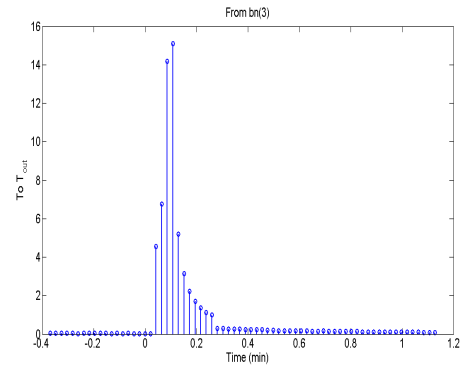
(a) F_f



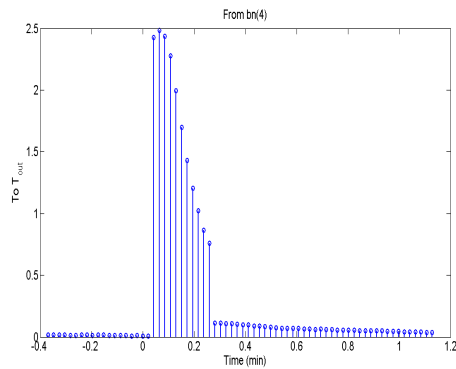
(b) $bn(1)$



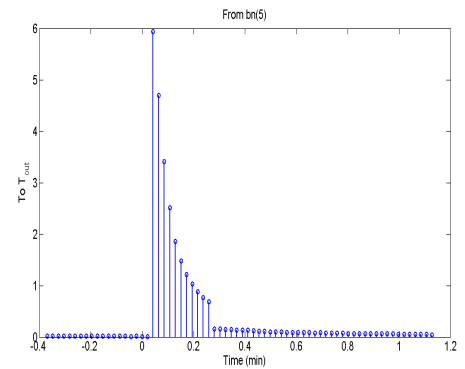
(c) $bn(2)$



(d) $bn(3)$

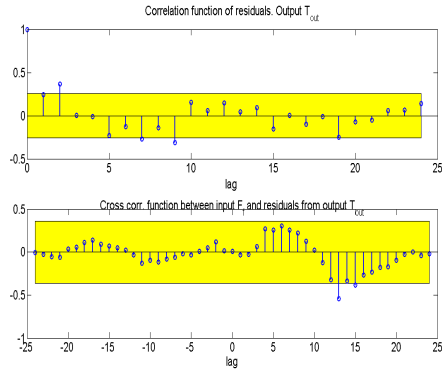


(e) $bn(4)$

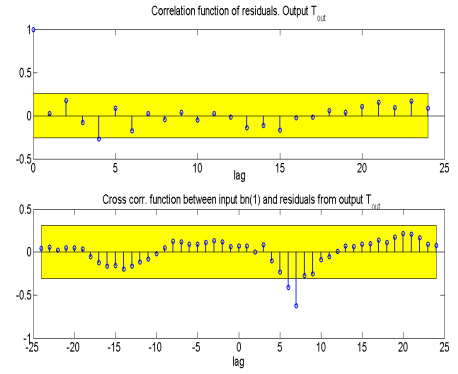


(f) $bn(5)$

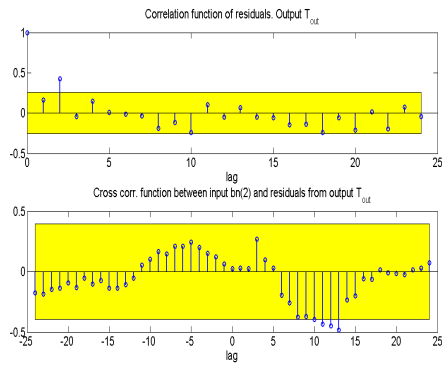
Figure 4.6: Tests of impulse response



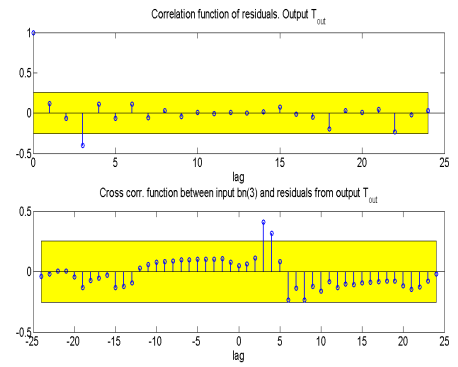
(a) F_f



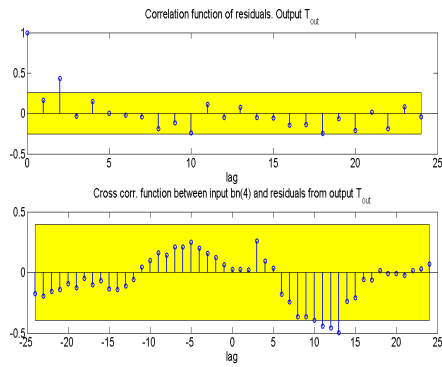
(b) $bn(1)$



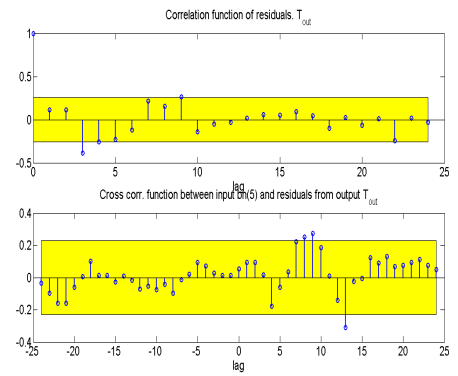
(c) $bn(2)$



(d) $bn(3)$

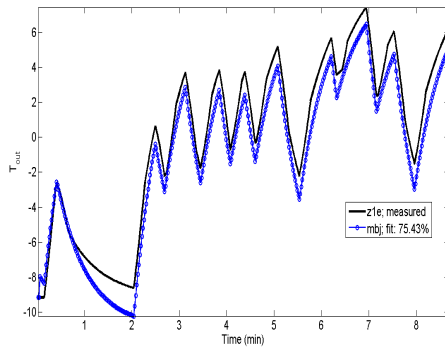


(e) $bn(4)$

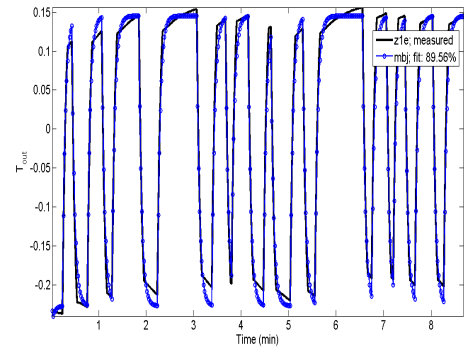


(f) $bn(5)$

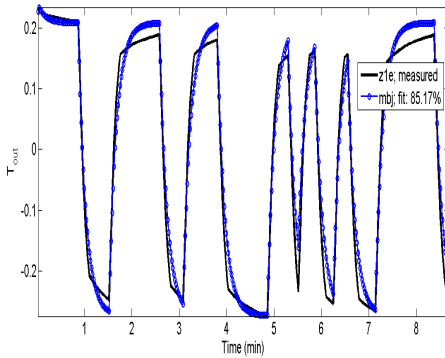
Figure 4.7: Residual tests



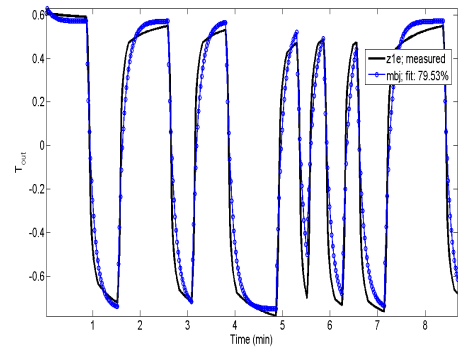
(a) F.f



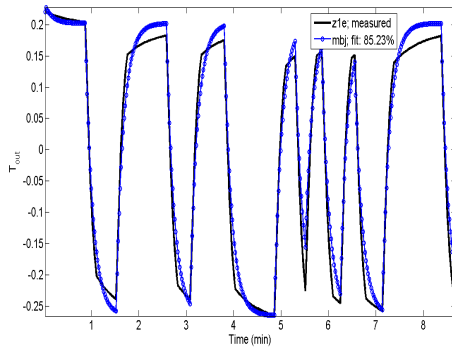
(b) bn(1)



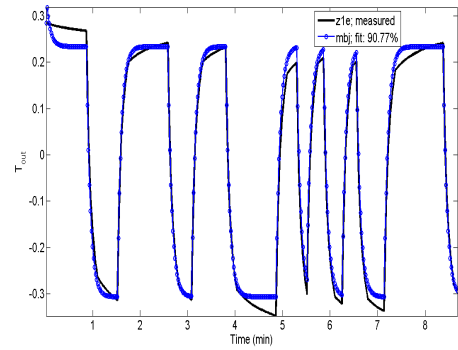
(c) bn(2)



(d) bn(3)

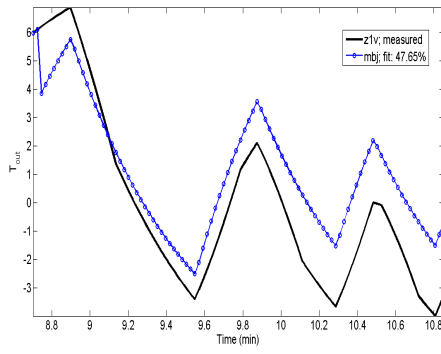


(e) bn(4)

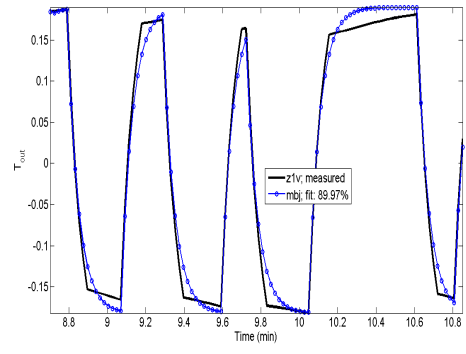


(f) bn(5)

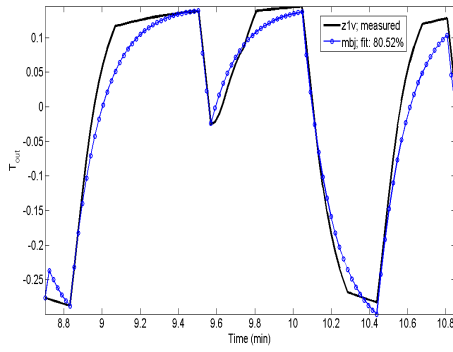
Figure 4.8: Infinite-step prediction performance



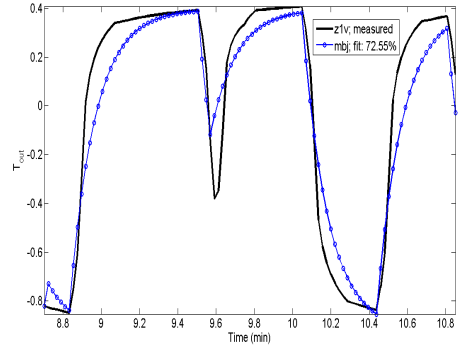
(a) F.f



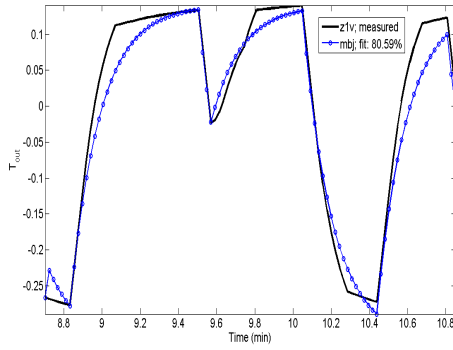
(b) bn(1)



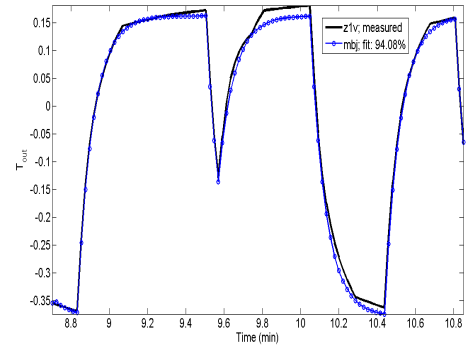
(c) bn(2)



(d) bn(3)



(e) bn(4)



(f) bn(5)

Figure 4.9: Infinite-step prediction validation

weight here the controller reacts too aggressively for disturbance changes and the results show oscillations.

A constraint function is written in Matlab to ensure the conventional MPC controller satisfy the following conditions:

$$J = \sum_{i=1}^{T_p} (\hat{y}(t_i) - r(t_i))^T Q(i) (\hat{y}(t_i) - r(t_i)) + \sum_{j=1}^{T_c} (u(t_j) - u(t_{j-1}))^T R(j) (u(t_j) - u(t_{j-1})) \quad (4.23)$$

s.t.

system's dynamic equations: Equation (4.21)

initial and boundary conditions: Equation (2.43) to Equation (2.52)

process constraints:

$$1700 \text{ scfm} \leq F_f \leq 1900 \text{ scfm} \quad (4.24)$$

$$0 \leq bn \leq 1 \quad (4.25)$$

The parameters in the objective functions such as prediction and control horizons and tuning parameters are the same as in Equation (4.17). Matlab function *fmincon* is used to calculate the constrained optimal control signals in this work. The Kalman filter supplies the MPC controller with states and also reduces the unwanted output noise. At each time interval, the state estimates are used as initial values of states in the control algorithm, in which the output prediction is calculated using the lumped discrete-time state-space model obtained using system identification approach. Set-point tracking response to a set-point change and regulatory behaviour in the presence of disturbance are studied in the following sections.

4.2.1 Set-point tracking

The output set-point tracking response of the primary gas reformer to a set-point change from 1105 K to 1100 K at time 6.5 min is evaluated.

From Figure 4.11, it can be seen that the outlet temperature tracks the set-point change smoothly with reasonable control action. The optimal control signals bring the system output to a new stable state within approximately 1.5 mins, which is about 3 residence time. As a result of the optimization, the obtained optimal control signals, fuel gas flow rate F_f and 5 burner states bn are presented.

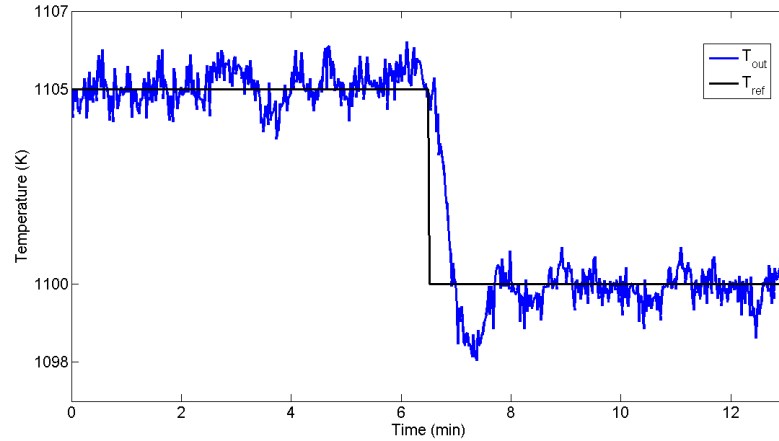


Figure 4.11: Set-point tracking response of the conventional MPC

Figure 4.12b and Figure 4.12a depict the profiles of obtained optimal control signals. It is noted that, in the controller design, the optimal control signals for burner states are assumed to be continuous variables that satisfy $bn \in [0 \ 1]$. It is an ideal value and may not be implemented in the on-line systems of the plants if the burners are manually operated. However, from Figure 4.12b, it is seen that during the stable states, the values of bn are either 0 or 1, reaching both upper and lower bounds of the constraint.

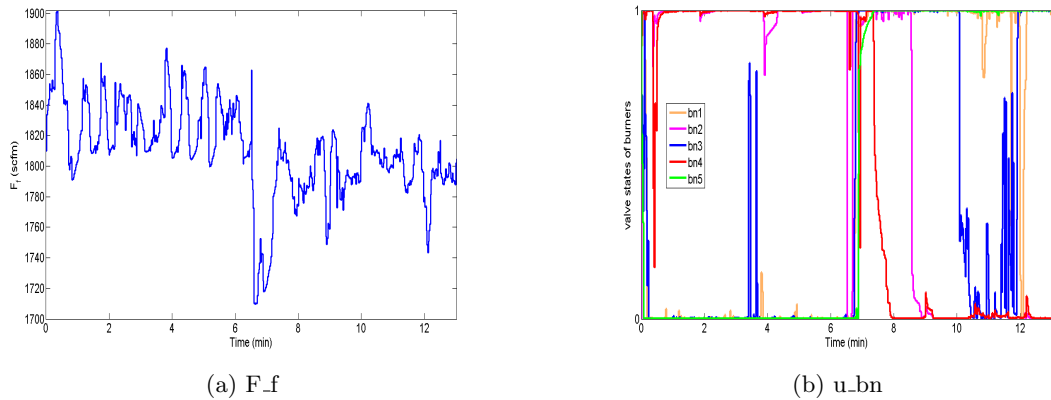


Figure 4.12: Control signals of fuel gas flow rate and burner states

In general, the result of set-point tracking response shows that the proposed conventional MPC controller using the lumped prediction model yields smooth and fast set-point tracking response with reasonable control action.

4.2.2 Regulatory behaviour

Figure 4.13 depicts the outlet temperature response to a disturbance change of the ambient temperature T_{amb} from $300K$ to $295K$ at 6.5 min .

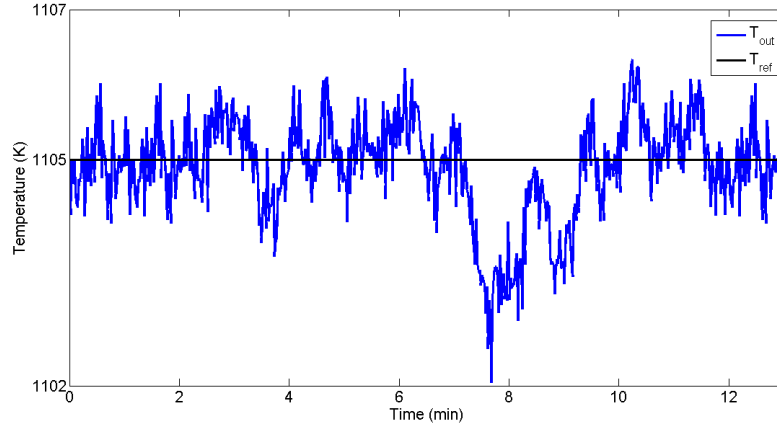


Figure 4.13: Set-point tracking response of the conventional MPC

From Figure 4.13, it can be seen that: from time 6.5 *min* to 7.7 *min*, the output deviates from the set-point for about three residence time due to the decrease of ambient temperature; from time 7.7 *min* to 8 *min*, the controller forces the output to track the set-point with corrective control action; from time 8 *min* to 10 *min*, the output diverges from the set-point due to plant-model mismatch, and then converges back to the set-point by the adjustment from the controller. The total time for the disturbance rejection behaviour is about 3.5 *min*, which is about 8 residence time.

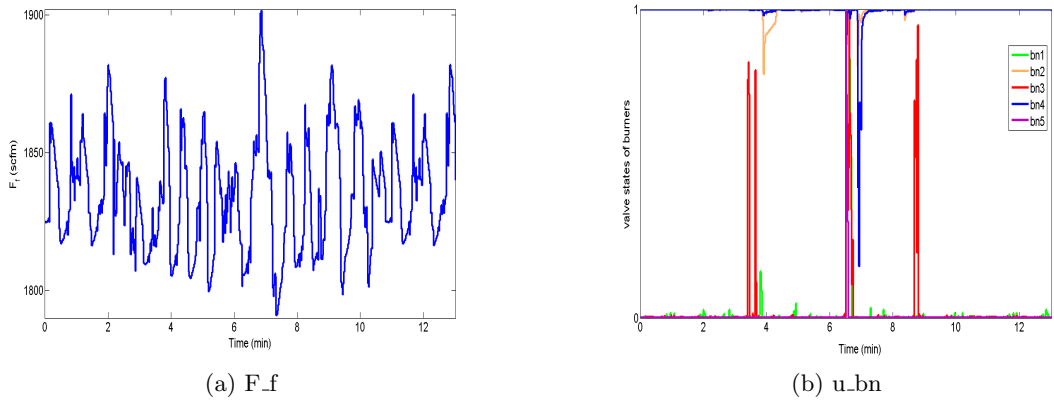


Figure 4.14: Control signals of fuel gas flow rate and burner states

Figure 4.14b and Figure 4.14a depict the profiles of obtained optimal control signals. From Figure 4.14b, it is seen that during the stable states, the values of bn are either 0 or 1, reaching both upper and lower bounds of the constraint. In general, the result of set-point tracking response shows that the proposed conventional MPC controller using the lumped prediction model yields relatively slow response in disturbance rejection with reasonable control action.

4.3 Conclusion

In this chapter, two predictive controllers are proposed based on late-lumping and early-lumping approximations of the DPS system respectively. In the design of MPC, the current control action is determined by solving a finite horizon open-loop optimal control problem on-line. Each optimization yields a control law that is applied to the plant until the next sampling instant. Constraints of states and inputs are directly enforced in the on-line optimal control problem. The two controllers have the same objective function and control algorithm with same parameter specifications (such as prediction and control horizons, tuning parameters, etc). But the number of inputs (burner states) in the two predictive controllers are slightly different and output noise is only introduced in one of the two controllers (the conventional controller), which makes the two predictive controllers incomparable. In CBMPC, full states are assumed to be measured exactly without error, so the state observer, which can handle noise rejection, is not designed. Non-linear state observer can be designed for CBMPC with introduced output noise in the future studies. In this section, performance of the two MPC controllers are evaluated, and further discussion about the difference between the two controllers are presented in regards to convergence time.

The following two figures provide general comparison of the simulation results of set-point tracking response to set-point change (see Figure 4.15) and disturbance rejection (see Figure 4.16).

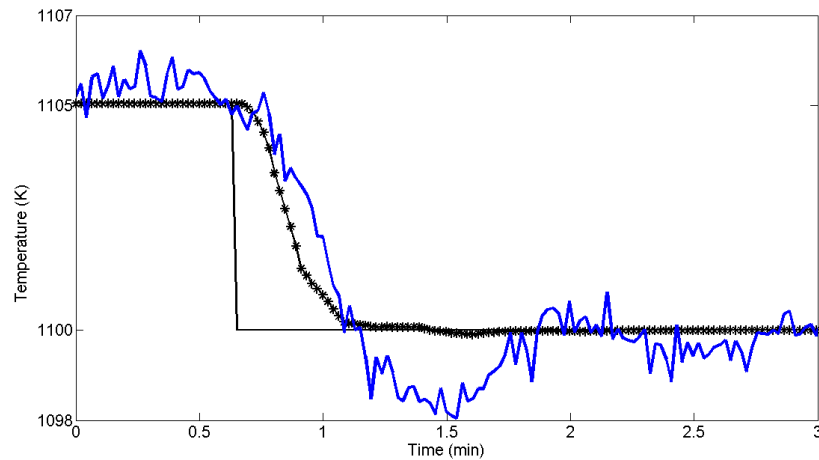


Figure 4.15: Performance comparison of two predictive controllers in set-point tracking

From Figure 4.15, it is seen that: 1) the output using CBMPC converged to the new state within 1 *min* (about 2 residence time); 2) the output using the conventional MPC converged to the new state within 1.5 *min* (about 3 residence time). The CBMPC yields faster set-point tracking response than the conventional MPC.

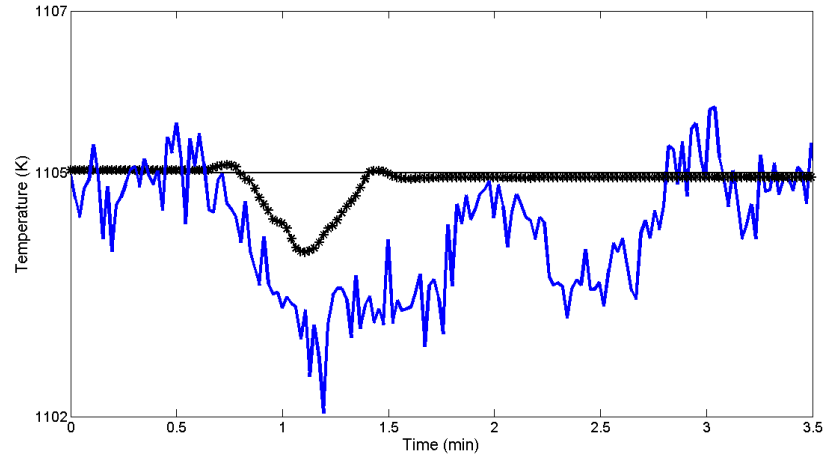


Figure 4.16: Performance comparison of two predictive controllers in disturbance rejection

From Figure 4.16, it is seen that: 1) the output using CBMPC converged to the new state within 1 *min* (about 2 residence time); 2) the output using the conventional MPC converged to the new state within 3.5 *min* (about 8 residence time). The CBMPC yields faster disturbance rejection performance than the conventional MPC.

The differences of the two predictive controllers are concluded as follows:

- One major difference is about the prediction model in its controller: CBMPC employs the late lumping approximation method, in which the distributed nature of the system is kept as long as possible in the course of control design, and numerical approximation techniques is required in the end due to computer implementation of the resulting control algorithms; the conventional MPC employs early lumping approximation, where the PDEs are approximated (lumped) first, and the control design proceeds with the lumped model equations (ODEs). The choice of the prediction model may directly affect accuracy of the calculation of the future states (model-plant mismatch) and further affect the convergence time and control accuracy.
- State observer is usually needed for the MPC design. In the conventional design, for the lumped **linear** prediction model developed by system identification method, Kalman filter is utilized for handling state estimation and measurement noise. However, in the CBMPC design, all states of the **non-linear** prediction model have their own physical meaning and are assumed to be all measured exactly without error (otherwise, a non-linear state observer is required), and no measurement noise is considered, thus no state observer is considered. This can be a limitation in on-line application.
- Theoretically speaking, the computational load for CBMPC is lower than any conventional MPC using early-lumping approximation approach because the method of

characteristics keeps the distributed nature of the system as long as possible in the course of control design, which saves lots of numerical on-line calculations compared to early-lumping approaches which enlarge the dimension of the model by discretizing PDEs to numerous ODEs. However, some of the parameters (such as the number of inputs, maximum numbers of the SQP iterations) in the control algorithms, which can also affect the computational load, are different, which makes the two predictive controllers incomparable in terms of computational load.

Chapter 5

Conclusions

In the previous chapters, the dynamic modelling and simulation of a primary gas reformer, the applications of steady state optimization and the design of model predictive controllers have been illustrated. This chapter reviews and discusses the key results and gives some suggestions for future research.

5.1 Summary

In this thesis, we have focused on the fulfilment of three goals:

- to develop a dynamic mathematical model that can describe the dynamic relationship between the synthesis gas outlet temperatures and the process variables consisting of manipulated and disturbance variables such as fuel gas flow rate, process gas flow rate, steam/carbon ratio, ambient temperature and burner states;
- to perform steady state optimization on an mixed-integer non-linear programming (MINLP) framework, aiming to improve the uniformity of synthesis gas temperatures from different tube reactors by manipulating side-fired burners;
- to design model predictive controllers for the dynamic distributed parameter system that regulate the production process accurately using two different approximation approaches (early-lumping and late-lumping).

First, background information about modelling partial differential equations and simulation techniques for distributed parameter systems were introduced in Chapter 1. It was shown that in an industrial system, the process can be described by the distributed parameter systems (DPS) interacted with the lumped parameter system (LPS) and supplementary algebraic equations (AEs). Before dynamic analysis, optimization and control design of such systems, it is a prerequisite to establish a mathematical model to describe the chemical processes of the system. Technical background information of related subjects (such as DPS, MINLP, MPC and method of characteristics) was also provided in Chapter 1.

We next developed the dynamic mathematical model for a primary gas reformer in Chapter 2. The reaction kinetics and heat transfer mechanisms involved in a side-fired primary gas reformer were investigated and the dynamic model was built based on three sub-models: tube-side model described by PDEs, furnace-side model described by ODEs and heat flux model described by AEs. In general, the dynamic model consists of four quasi-linear PDEs and two ODEs accompanied by numerous supplementary AEs. Model parameters were further tuned against empirical data. Numerical outputs of model simulations and measured data recorded from an ammonia plant were compared and good agreement was found in both trends and absolute values. The steady state modelling and analysis of a primary reformer using energy balance equations were performed considering simultaneous radiation and convection heat transfer processes and chemical reforming reactions in the presence of catalyst. The comparison of computed and measured data showed the importance of parameters such as feed flow rate, steam/carbon ratio, fuel gas flow rate, and ambient temperature in methane conversion efficiency. Dynamic simulation on step changes had also provided information for input design for applying system identification methods.

Using the dynamic model built in Chapter 2, an mixed-integer non-linear programming (MINLP) based optimisation framework was developed in gPROMS in Chapter 3, with four proposed objective functions focusing on the improvement of the uniformity of temperatures (process gas or tube wall temperatures) from different tube reactors. The dynamic process model was first computed until it reached stable steady states. MINLP based optimisation solver using outer approximation algorithm was then implemented for steady state optimization. Obviously, objective functions were significantly reduced after the decision variables were moved towards the optimal status. Differences among outlet temperatures at different locations were reduced as well. The optimization results of burner states from objective function of tube wall temperatures with outlet temperature constraint yields to relatively smooth and uniformed heat flux profile, which may help prolong the service time of the equipments.

Chapter 4 presented the simulation results of two predictive controllers are proposed based on late-lumping (CBMPC) and early-lumping (a conventional MPC) approximations of the DPS system respectively. The control objective was to meet a set-point for the process gas outlet temperature by manipulating the fuel gas flow rate and burner states. Set-point tracking and disturbance rejection performances of the two MPC controllers were evaluated. It was demonstrated that both predictive controllers were capable of providing satisfactory performance, while CBMPC yielded a much shorter convergence time. Difference between the two controllers were further presented and discussed.

5.2 Future Work

Throughout the entire thesis, we have been concentrating on the dynamic mathematical modelling, optimization and optimal control design of a primary gas reformer. In this section, we would like to share our perspectives on the directions and fields that are worthy of future investigations:

- In this thesis, all discussions on controller design of the system were based on discrete monitor output. However, actual monitor outputs can be continuous. The sampling time $t_s = \frac{L}{mu_i}$ was fixed in this work, however, can be varying if operating condition changes. Implementations of dynamic control system with time-varying sampling intervals is worth further study.
- The control horizon and prediction horizon in the model predictive control algorithm were fixed for both MPC controllers. By tuning control horizon and prediction horizon can help us find the most efficient way to obtain the most accurate and time-saving results.
- In Chapter 4, the predictive controllers were built based on controlling the outlet temperature of one tube reactor; while in industrial cases, hundreds of tubes are installed in the reforming furnace, which may make this method not suitable for large scale problems. More studies of simplifying calculation process while maintaining the distributed nature of the system is desired for large scale problems.
- In the conventional MPC design, system identification is used as the early-lumping approximation method. Finite difference approximation method is also a popular method as an early-lumping approximation and is worth further investigation.
- In regards to the computational load, the comparison between predictive controllers based on early-lumping and late-lumping approximations can also be further studied if we introduced output noise and designed a state observer in the CBMPC.

Bibliography

- [1] A. A. Alhaddad and G. A. Coulman. Experimental and theoretical study of heat transfer in pulse combustion heaters. In *Proceedings Vol. I: Symposium on Pulse Combustion Applications*, GRI-8210009.2, Atlanta. GA, 1982.
- [2] V. I. Arnold. *Geometric Methods in the Theory of Ordinary Differential Equations*. Springer-Verlag, 1988.
- [3] M.S. Bazaraa and C.M. Shetty. *Nonlinear Programming: Theory and Algorithms*. John Wiley & Sons, 1979.
- [4] E. M. L. Beale. *Numerical Methods In: Nonlinear Programming*. North-Holland Publishing Co, Amsterdam, 1967.
- [5] B. Wayne Bequette. *Process Dynamics Modeling, Analysis, and Simulation*. Prentice Hall PTR, 1998.
- [6] A. Burghardt and J. Aerts. Pressure changes during diffusion with chemical reaction in a porous pellet. *Chem. Eng. Proc.*, 1988.
- [7] T. Anderson C. Thomas and T. Hill. Life assessment of reformer tubes from strain measurement. *NACE International: Corrosion 2011 Conference & Expo*, 2011.
- [8] P. D. Christofides. *Nonlinear and Robust Control of PDE Systems: Methods and Applications to Transport-Reaction Processes*. Birkhuser Basel, 2001.
- [9] P. D. Christofides and P. Daoutidis. Feedback control of hyperbolic pde systems. *AIChE Journal*, 34:557, 1995.
- [10] P. D. Christofides and P. Daoutidis. Robust control of hyperbolic pde systems. *Chem. Eng. Sci.*, 53:85, 1998.
- [11] Joseph Colannino. Ethylene furnace heat flux correlation. Technical report, John Zink Company LLC, 2008.
- [12] B. J. Cromarty. Reformer tubes failure mechanisms, inspection methods and repair techniques. In *Johnson-Matthey 12th annual international technical seminar on hydrogen plant operations*, 2004.
- [13] P. Duchateau and D. Zachmann. *Applied Partial Differential Equations*. Harper & Row Publisher, 1989.
- [14] M.A. Duran and I.E. Grossmann. A mixed-integer nonlinear programming approach for process systems synthesis. *AIChE Journal*, 32(4):592–606, 1986.
- [15] M.A. Duran and I.E. Grossmann. An outer-approximation algorithm for a class of mixed-integer nonlinear programs. *Mathematical Programming*, 36:307–339, 1986.
- [16] Y. A. engel and Boles. *Thermodynamics : An Engineering Approach 4th Edition*. McGraw-Hill, 2001.

- [17] S. Ergun and A.A. Orning. Fluid flow through packed columns. *Chemical Engineering Progress*, 48:89–94, 1952.
- [18] Lim Yueh Yang et al. Production of hydrogen via syngas route. Technical report, National University of Singapore, 2007/2008.
- [19] R. Fletcher. *Practical Methods of Optimization*. Wiley, Chichester, 1987.
- [20] R. Fletcher and S. Leyffer. Solving mixed integer nonlinear programs by outer approximation. *Mathematical Programming*, 66:327–349, 1996.
- [21] C.A. Floudas. *Nonlinear and Mixed-Integer Optimization: Fundamentals and Applications*. Oxford University Press, 1995.
- [22] David N. French. Creep and creep failures. Technical report, The National Board of Boiler and Pressure Vessel Inspectors, Northborough, MA, 1991. <http://www.nationalboard.org/Index.aspx?pageID=181>.
- [23] M. J. Goldsmith. *Sequential Quadratic Programming Methods Based on Indefinite Hessian Approximations*. PhD thesis, Stanford University, 1999.
- [24] I.E. Grossmann. Review of nonlinear mixed-integer and disjunctive programming techniques. *Optimization and Engineering*, 3:227–252, 2002.
- [25] J.F. Forbes H. Shang and M. Guay. Model predictive control for quasilinear hyperbolic distributed parameter systems. *Ind. Eng. Chem. Res.*, 2004.
- [26] J.F. Forbes H. Shang and M. Guay. Feedback control of hyperbolic distributed parameter systems. *Chemical Engineering Science*, 2005.
- [27] J.F. Forbes H. Shang and M. Guay. Computationally efficient model predictive control for convection dominated parabolic systems. *Journal of Process Control*, 2007.
- [28] E. M. Hanczyc and A. Palazoglu. Sliding mode control of nonlinear distributed parameter chemical processes. *Ind. Eng. Chem. Res.*, 34:557, 1995.
- [29] E.M. Hanczyc and A. Palazoglu. Nonlinear control of a distributed parameter process: the case of multiple characteristics. *Industrial Engineering & Chemistry Research*, 1995.
- [30] B. Huang and R. Kadali. *Dynamic Modeling, Predictive Control, and Performance Monitoring*. Springer-Verlag, 2008.
- [31] I.M. Alatiqi and A.M. Meziou. Dynamic simulation and adaptive control of an industrial steam gas reformer. *computers chemical engineering*, 15(3):147–155, 1991.
- [32] I. Karafyllis and P. Daoutidis. Control of hot spots in plug flow reactors. *Computer & Chemical Engineering*, 2002.
- [33] Ali Sener Kaya. On the optimal operation of the open plate reactor. Master’s thesis, Dalarna University, 2007.
- [34] J.P.G. Kehoe and R. Aris. Communications on the theory of diffusion and reaction ix. internal pressure and forced flow for reactions with volume change. *Chem. Eng. Sci.*, 1973.
- [35] G.R. Kocis and I.E. Grossmann. Global optimization of nonconvex minlp problems in process synthesis. *Industrial & Engineering Chemistry Research*, 27:1407–1421, 1988.
- [36] Dean Latham. Mathematical modelling of an industrial steam methane reformer. Master’s thesis, Queen’s University, 2008.
- [37] Sven Leyffer. *Deterministic Methods for Mixed Integer Nonlinear Programming*. PhD thesis, University of Dundee, 1993.

- [38] L. Ljung. *System Identification: Theory for the User*. Prentice-Hall, 2 edition, 1999.
- [39] A. Maida and J. P. Corriou. Boundary control of nonlinear distributed parameter systems by input-output linearization. In *18th IFAC World Congress Milano*, Italy, 2011. International Federation of Automatic Control (IFAC).
- [40] MATLAB. *Version 7.13 (R2011b)*. The MathWorks Inc., Natick, Massachusetts, 2011.
- [41] R. McOwen. *Partial Differential Equations*. Prentice Hall Inc.: Upper Saddle River, 1996.
- [42] M.P.Sukumaran Nair. Ammonia industry-today and tomorrow. Technical report, Petrochemical developments, 2006.
- [43] Dias M.M. Nan H.S. and Rodrigues A.E. Effect of forced convection on reaction with mole changes in porous catalyst. *Chem. Eng. J.*, 1995.
- [44] NYSERDA. Hydrogen fact sheet: Hydrogen productionsteam methane reforming (smr). Technical report, New York State Energy Research and Development Authority, 2008.
- [45] C.E.G. Padro and V. Putsche. Survey of the economics of hydrogen technologies. national renewable energy laboratory. Technical report, National Renewable Energy Laboratory, USA, 1999.
- [46] M.A. Saunders P.E. Gill, W. Murray and M.H. Wright. Constrained nonlinear programming. *Handbooks in Operations Research and Management Science*, 1, Optimization:171–210, 1989.
- [47] PSE. *gPROMS Advanced User Guide*. Process Systems Enterprise Ltd., Bridge Studios, 107a Hammersmith Bridge Road, London W6 9DA, United Kingdom, 2004.
- [48] PSE. *gPROMS Introductory User Guide*. Process Systems Enterprise Ltd., 2004.
- [49] W. H. Ray. *Advanced Process Control*. Butterworth-Heinemann, 1989.
- [50] R. D. Roberts and J. Brightling. All inclusive approach for steam reformers inspection methods. *The e-Journal of Nondestructive Testing*, 2005.
- [51] Christiansen L.J. Rostrup-Nielsen J.R. and Bak Hansen J. H. Activity of steam reforming catalysts: Role and assessment. *Allied Catalysis*, 43:287–303, 1988.
- [52] Berc Rustem. *Algorithms for Nonlinear Programming & Multiple Objective Decisions*. John Wiley, 1998.
- [53] N.H. El-Farra S. Dubljevic, P. Mhaskar and P. Christofides. Predictive control of transport reaction processes. *Computers & Chemical Engineering*, 2005.
- [54] Karel Schnebele. Fuel cell reformer control design. Technical report, Rensselaer Polytechnic Institute, 2006.
- [55] H. Shang. *Characteristic-based control of distributed parameter systems*. PhD thesis, University of Alberta, 2003.
- [56] H. Sira-Ramirez. Distributed sliding mode control in systems described by quasilinear partial differential equations. *System and Control Letters*, 1989.
- [57] T. Soderstrom and P. Stoica. *System Identification*. Prentice-Hall, 1989.
- [58] J. E. Thomas. *Fundamentals of Petroleum Engineering*. Ed. Intercincia, Petrobrs, 2004.
- [59] A. Thowsen and W.R. Perkins. Optimal discrete time feedback control of mixed distributed and lumped parameter systems. *International Journal of Control*, 1973.

- [60] A. Thowsen and W.R. Perkins. Sampled-data linear-quadratic regulator for systems with generalized transportation lags. *International Journal of Control*, 1975.
- [61] J. G. VanAntwerp and R. D. Braatz. Model predictive control of large scale processes. *J. of Process Control*, 2000.
- [62] Versteg G.F. Veldsink J.W., Van Damme R.M.J. and Van Swaaij W.P.M. The use of dusty-gas model for the description of mass transport with chemical reaction in porous media. *Chem. Eng. J.*, 1995.
- [63] Margrete Hnes Wesenberg. *Gas Heated Steam Reformer Modelling*. PhD thesis, Norwegian University of Science and Technology, April 2006.
- [64] R. B. Wilson. *A simplicial algorithm for concave programming*. PhD thesis, Harvard Univ. Graduate School of Business Administration, 1960.
- [65] A. V. Wouwer. Modelling and simulation of distributed parameter systems. *Control Systems, Robotics and Automation*, 2003.
- [66] Jianguo Xu and Gilbert F. Froment. Methane steam reforming, methanation and water-gas shift: I. intrinsic kinetics. *AIChE Journal*, 35(1):88–96, 1989.